Transparent Superhydrophobic Polycarbonate Coating

A Thesis Presented for the
Master of Science
Degree
The University of Tennessee, Knoxville

Gimgun Loi
May 2015

Copyright © 2015 by Gimgun Loi.
All rights reserved.

DEDICATION

I would like to dedicate this work to the department of Materials science and Engineering at the University of Tennessee. Everyone has been a great help and has truly helped me succeed and I could have asked for a better department with better people. I would also like to dedicate this work to my mother for all the endless support and guidance she has given me through my whole life. Thank you to everyone who helped me through this journey.

ACKNOWLEDGEMENTS

I would like to thank my advisor Dr. Roberto Benson for all his patience, guidance and support through this project. I have learned so much from him and I couldn't ask for a better advisor. I would also like to thank Dr. David Harper and Dr. John Simpson for also advising me through this project. I would also like to thank Steve McNeany, Greg Jones, Chris Wettland, and Dr. Omid Hosseinaei for assisting me with any problems I may have encountered through this work. Lastly I would also like to thank the Center of Materials Processing for funding me.

ABSTRACT

Superhydrophobicity is a property commonly seen in nature such as the lotus leaf. This unique property allows the surface of a material to exhibit water repellency and self-cleaning abilities. This effect is contributed by two important components: the rough surface topography and low surface free energy. Since the discovery of this unique property, several methods and various materials have been used to produce this effect and used in a wide variety of applications. However, the use of this type of effect on transparent surfaces is still being researched. I have proposed a method to develop a transparent superhydrophobic coating using a transparent polymer such as Polycarbonate (PC) as a matrix . Functionalized aerogel particles are broken down to nanosized particles by milling and sonication, and added into solution with PC. This solution is then applied on various substrates such as quartz and silicon wafers though a spin coating process. The film produced is transparent with a transmission of 92-93%. The increase in coating thickness showed only a slight reduction in the transmission; however, the transmission still exhibited an equal or higher transmission than observed for quartz glass without a coating. The superhydrophobic properties were obtained based on contact angle measurements of 150° or greater, which represent a combination of low surface free energy and nano-textured topography of the coating. Another important aspect to achieving a superhydrophobic coating is the addition of a rough surface topography. The SEM and AFM measurement indicates that the superhydrophobic polycarbonate coating (SHPC) coating exhibits the rough nano-textured topography for obtaining superhydrophobicity. The mechanical properties of the film indicated a decrease in hardness and modulus with the increase of the coating thickness, which is influenced by the substrate. This method has shown to be a simple and effective method that can be applied to a variety of substrates and can be expanded to being used for coating larger surfaces through different methods, such as spray coating. The coating has the potential to be used for various transparent applications, such as camera lenses, windows, and solar panels.

TABLE OF CONTENTS

CHAPTER I Introduction **1**

CHAPTER II Background **3**
2.1 Superhydrophobic Fundamental Theory **3**
2.1.1 Surface Free Energy 3
2.1.2 Surface Roughness 6
2.2 Superhydrophobic Surfaces **9**
2.2.1 Natural Superhydrophobic Surfaces 9
2.3.1 Properties and Applications 16
2.3 Polycarbonate (PC) **16**
2.3.1 Introduction to Polymers 16
2.3.2 Properties and Applications 18
2.3.4 Polycarbonate Degradation 19
2.4 Transparency and Optics **21**
2.4.1 Introduction to Optics 22
2.4.2 Shell's law 23

CHAPTER III Materials and Methods **25**
3.1 Development of Coating **25**
3.1.1 Materials 25
3.1.2 Preparation of coating solution 25
3.1.3 Spin Coating 25
3.2 Characterization **26**

CHAPTER IV Results **29**
5.1 Surface Chemistry and Topography **29**
5.1.1 Elemental and Functional group analysis 29
5.1.2 Surface Micrographs (SEM) 31
5.1.3 Surface topography (AFM) 45
5.1.4 Thickness of the Coating 48
5.2 Superhydrophobicity **52**
5.2.1 Contact Angle Measurement 52
5.3 Optical Properties **54**
5.3.1 Transmission 54
5.4 Mechanical Properties **55**
5.4.1 Nanoindentation 55

CHAPTER V Discussion **58**

CHAPTER VI Conclusions and Future Work **66**
6.1 Conclusions **66**
6.2 Future Work **66**

LIST OF REFERENCES **68**

APPENDIX **71**

VITA **76**

LIST OF TABLES

Table 1: BPA-PC properties using various testing standard [44] 19
Table 2: The minimum and maximum peak heights in the coating and the average roughness of the SHPC coatings. 47
Table 3. Contact Angle measurement of the SHPC coatings at five different points. 52
Table 4: The Surface free energy obtained through contact angle measurements and the work of adhesion between the liquid and the solid 54
Table 5: The depth of penetration for EDS compared to the Thickness of the SHPC 1X and SHPC 10X coatings. 59
Table 6: The calculated depth of penetration for ATR 60
Table 7: Estimated surface free energy and work of adhesion for SHPC 10X . 65
Table 8: The EDS chemical composition for SHPC 1X and SHPC 10X 72
Table 9: The calculated surface free energy 74
Table 10: Estimated adhesion strength 74

LIST OF FIGURES

Figure 1 : The chemical structure of PTFE 6
Figure 2: The Wenzel Model [11] 7
Figure 3: The Cassie-Baxter Model [11] 8
Figure 4: SEM images of the Lotus Leaf [10]. 10
Figure 5: SEM images of *Planipennia* a species of insect with lace wings similar to that of mayflies and dragonflies [19] 11
Figure 6: The SEM image of the superhydrophobic legs of *Gerris remigis* commonly known as water sliders [17]. 11
Figure 7: The SEM image of the superhydrophobic wings of *Cicada orni* commonly referred to as cicades[18]. 12
Figure 8: LbL method for producing superhydrophobic surfaces by applying nanoparticles with functional groups (A and C) are layered on top of the substrate and combined to form B functional groups that covalently joins the layers [30]. 14
Figure 9: SEM images of PP-PMMA in a DMF solution a) with a concentration of $1x10^{-4}$ g m L^{-1} and b) with a concentration of $5x10^{-4}$ g m L^{-1} [33] 15
Figure 10: The difference in contact angle measured of a poly(butyl methacrylate-co-ethylene dimethacrylate nonporous and porous along with the SEM images of a superhydrophobic porous polymer [34] 15
Figure 11: The relationship between structure, properties, and processing 17
Figure 12: Polycarbonate chemical structure 18
Figure 13: Photo-Fries Mechanism [48] 20
Figure 14: Photo- Oxidation Mechanism of PC [48]. 21
Figure 15: The Electromagnetic Spectrum [43]. 22
Figure 16: Shell's Law 24
Figure 17: Five points were measured for the CA for the SHPC coating 27
Figure 18: EDS spectrum of SHPC 1X coating on a silicon wafer at 1863X. 30
Figure 19: EDS spectrum of the SHPC 10X coating on a silicon wafer at 3728X. 30
Figure 20: The FTIR spectrum of SHPC 10X coating on a silicon wafer using ATR. 31
Figure 21: The SEM micrographs of SHPC 1X coating on a silicon wafer at a) 10KX, b) 25KX, and c) 100KX with indication of coating distribution. 33
Figure 22: The SEM micrographs of SHPC 3X coating on a silicon wafer at a) 10KX, b) 25KX, and c) 100KX with indication of coating distributions 36
Figure 23: The SEM micrographs of SHPC 5X coating on a silicon wafer at a) 10KX, b) 25KX, and c) 100KX with indication of coating distribution. 39

Figure 24: SEM images of (a) SHPC 1X (b) SHPC 3X (c) SHPC 5x coating on a silicon wafer at a 100KX magnification for relative pore size distribution. 42
Figure 25: AFM images of SHPC 1X coating on a silicon wafer in a 10μm by 10μm area. 45
Figure 26: AFM images of SHPC 3X coating on a silicon wafer in a 10μm by 10μm area. 46
Figure 27: AFM images of SHPC 5X coating on a silicon wafer in a 10μm by 10μm area. 46
Figure 28: Histogram of the roughness of the SHPC coatings. 47
Figure 29: SEM images of (a) SHPC 1X (b) SHPC 3X and (c) SHPC 5X coating on a silicon wafer observed at 100KX. 49
Figure 30: Contact Angle Measurement of different number of coatings with DI water and Diiodomethane probe liquids. 53
Figure 31: Superhydrophobic polycarbonate coating (SHPC) coated 10 times on a quartz substrate with water rolling off the surface. 53
Figure 32: Transmission of SHPC coatings on quartz glass through the visible light range. 55
Figure 33: Young's modulus obtained for SHPC 3X, SHPC 5X, and SHPC 10X coating on silicon wafer. 56
Figure 34: Hardness obtained for SHPC 3X, SHPC 5X, and SHPC 10X coating on silicon wafer. 57
Figure 35: An illustration of the SHPC coating when water is on the surface 62
Figure 36: The transmission of the SHPC coatings from 800nm to 200nm. 73
Figure 37: The reduced modulus obtained from nanoindentation on the SHPC coatings 75

CHAPTER I
INTRODUCTION

Superhydrophobicity is the property of extreme water-repellency of a surface. This unique property has been studied vastly and has various applications such as self-cleaning windows and water repellant coatings on numerous substrates. This unique property was first discovered in nature on the leaves of plants such as the lotus leaf, thus this property is also commonly known as the “lotus effect”. It was speculated that the surface of these leaves were water repellant, keeping them dry and clean. Similar effects were observed on various insect components such as the wings and legs. The exploration of the lotus leaf revealed two essential required components to achieve a superhydrophobic surface: low surface free energy and rough surface topography. This speculation inspired the pursuit of developing synthetic superhydrophobic surfaces, which has been achieved through methods such as chemical vapor deposition, layer-by-layer deposition, and phase separation processes [20-31]. The most commonly known superhydrophobic coating in the market is NeverWet, which uses functionalized silicon nano-particles. The development of these superhydrophobic surfaces could then applied for a wide range of applications such as self-cleaning applications, anti-biofouling, anti-corrosion, and anti-icing applications.

Although there has been much success in the development of superhydrophobic coatings, there still remains a need for an optically transparent superhydrophobic surface. A transparent superhydrophobic coating can be applied to windows, camera lenses, and solar panels for water repellent and self-cleaning capabilities. Light transparency is characterized by having a transmission through a material in the visible light wavelength range from 700nm to 400nm. The superhydrophobic surface property incorporates a rough surface topography ranging in the micro-nano range. It has been difficult to combine the rough surface topography of superhydrophobic coatings with optical transparency on one surface due to the large particle used for superhydrophobic coating acting as scattering centers preventing optical transmission. Attempting to decrease the surface roughness to the nano-scale range to achieve these transparent superhydrophobic surfaces is theoretically feasible; however, there are inhalation dangerous associated with the use of nano-size powders. Thus, to avoid the release of nano-particles oxides into the air, the particles must be embedded in a matrix.

Polymers are a material class that has shown to have extensive uses in various fields and can be found in nature or synthetically produced. This material class is unique due to its wide range of different properties such as impact resistance, elasticity, corrosion resistant, etc. tailored for each specific application. Polymers can also be easily processed through extrusion, injection molding, and solution casting. Polycarbonate (PC) is an amorphous transparent polymer that easily dissolves in tetrahydrofuran (THF) to form a solution. This optically transparent polymer would be an ideal substrate for embedding superhydrophobic nanoparticles into the surface to produce a transparent superhydrophobic surface.

This study introduces a simple and effective method to produce a polymeric based transparent superhydrophobic coating that can be applied on quartz and silicon wafer substrates. This coating will utilize functionalized aerogel nanoparticles embedded in a PC matrix. A solution with PC and aerogel can then be applied to surfaces using spin coating. Confirmation of the superhydrophobic components (low surface free energy and rough surface topography) will be explored for the superhydrophobic polycarbonate coating (SHPC) using energy dispersive spectroscopy (EDS), Fourier transform infrared spectroscopy (FTIR), atomic force microscopy (AFM), and scanning electron microscopy (SEM). Elemental analysis using EDS will identify the elements present in the coating to confirm the presences of PC and aerogel as well as the composition of each element. Aerogel is naturally composed of SiO_2, which is a hydrophilic material and thus using FTIR with attenuate total reflectance (ATR) will be used to confirm functionalization to obtain hydrophobicity. Using the SEM, the surface of the SHPC coatings will be observed with different thickness to correlate the coverage with the superhydrophobicity of the coatings. AFM will also be measured for the SHPC coatings to obtain the thickness of the coating with the addition of layers and to obtain the average roughness with the increase in layers. Contact angle measurements (CA) will be measured for each coating to measure the superhydrophobicity of the coating and to calculate the surface free energy and work of adhesion of the SHPC coating. To confirm the optical transparency of the SHPC coatings, transmission will be measured and compared to the transmission of quartz. Nanoindentation will be measured to obtain the hardness and modulus of the coating for a better understanding of the mechanical properties.

CHAPTER II
BACKGROUND

2.1 Superhydrophobic Fundamental Theory

2.1.1 Surface Free Energy

When a liquid droplet interacts with the surface of a substrate, the liquid will either spread out or bead up depending on the surface free energy. A substrate with a lower surface free energy will cause the liquid to bead up creating fewer interactions with the surface; while surfaces with higher energy would tend to spread onto the surface creating larger interactions [1]. The surface free energy is an excess of energy on the surface in a solid or liquid due to unbalanced molecular forces that accumulates on the surface [2]. In liquids, the surface free energy can be observed by the reduction in surface area due to internal forces; however, in solids it is more difficult to observe due to the lack of mobility. The wettability is associated with the surface free energy of two phases, such as a solid and liquid interacting, producing an additional energy known as interfacial free energy [2]. The interfacial free energy is the additional energy produced from the interaction between two condensed phases [2]. Polar and nonpolar interactions can often be separated into hydrophilic or hydrophobic interactions. Hydrophobic interactions can often be described as non-polar interactions that occur due to the small difference in electronegativity between the two interacting atoms. Hydrophilic interactions, also known as polar interactions, has the opposite effect in which the difference in electronegativity is quite large causing a larger dipole-moment creating a bond between two atoms.

The surface free energy of a substrate can be obtained through Young's equation (Eq.1), which incorporates a measured contact angle between solid-liquid interface

$$\cos\theta = \frac{(\gamma_s - \gamma_{sl})}{\gamma_l} \qquad (1)$$

where θ is the contact angle of a liquid placed on a surface, γ_s and γ_l are the surface tensions of the solid and liquid, and γ_{sl} is the interfacial free energy from

the solid and the liquid [3]. This equation is applicable to flat static surfaces with no surface roughness; however, the idea of a completely smooth surface is not ideal and surface roughness must be accounted for using models developed by Wenzel and Cassie-Baxter [4, 5].

The work of adhesion (W_a) is the energy between the surfaces to the liquid can be seen in Equation 2. This is equivalent to the energy required to separate the solid-liquid interface [6]. Incorporating this equation into Young's equation creates the Young-Dupree equation (Equation 3) that can be utilized to obtain the surface free energy of the solid by associating the contact angle and the surface tension of the probe liquids.

$$Wa = \gamma_l + \gamma_s + \gamma_{ls} \tag{2}$$

$$Wa = \gamma_l (1 + \cos\theta) \tag{3}$$

There are several methods proposed to obtaining the surface free energy of the solid; however, Wu's method has proven to be more reliable and exact [6, 7]. Wu's method to calculate surface free energy is introduced in Equation 4-6:

$$\gamma_l = \gamma_l^d + \gamma_l^p \tag{4}$$

$$\gamma_s = \gamma_s^d + \gamma_s^p \tag{5}$$

$$\gamma_{sl} = \gamma_l + \gamma_s - 4\left(\frac{\gamma_l^d \gamma_s^d}{\gamma_l^d + \gamma_s^d}\right) - 4\left(\frac{\gamma_l^p \gamma_s^p}{\gamma_l^p + \gamma_s^p}\right) \tag{6}$$

where γ_l^d and γ_l^p is the dispersive and polar component for the surface tension of the liquid and γ_s^d and γ_s^p is the dispersive and polar component for the surface free energy of the solid. This method is an expansion on Fowkes method that describes that the interfacial tension is caused by the two surface tensions γ_s and γ_l. The surface tension is resulted from dispersive interaction and polar interactions that can be described as a geometric mean [6]. A geometric mean is

an average that retains a reoccurring value from the product of their values, which can be described by Equation 7

$$\phi^{d} = \left(\gamma_1^{d}\gamma_2^{d}\right) \tag{7}$$

where ϕ^{d} is the interaction term for the dispersive energy, γ_1^{d} is the polar component of the surface tension of one phase and γ_2^{d} is the polar component of the surface tension of the other phase. A similar equation can be seen for the interaction term for the polar energy. In Wu's method the same concept is applied; however, the interactions are described as a reciprocal mean and has been proven to have more accurate results than Fowkes method [6, 7]. Wu's method accounts for the effects of polarities between two phases. When the polarities between two phases are similar the interfacial tension will be lower. Wu compared his method to Fowkes and resulted in values closer to the surface tension of polytetrafluoroethylene (PTFE) and polycholortrifuloroethylene (PCTFE) than that using Fowkes method [6].

The functional groups of the surface are an important contribution to the surface free energy, as some surfaces have been proven to have lower surface free energy than others. The difference is due to the available bonds present on the surface as compared to the bulk that allows it to form interactions such as hydrogen bonds that is more energetically favorable to relieve the surface tension of the liquid than internal forces [8]. This can easily be observed with water on glass. A commonly known hydrophobic material is Teflon, which measures to have a contact angle of 100° without roughening of the surface [9]. Teflon is the commercial name for polytetrafluoroethylene (PTFE) and has been used for a wide variety of applications due to its unique properties. The chemical structure of PTFE (Figure 1) is composed of fluorocarbons. Fluorine is a halogen and thus only has one remaining electron position to be filled. This makes it extremely electronegative, which results in forming covalent bonds to the carbon. These fluorine groups present on the surfaces cannot form hydrogen bonds and thus water does not wet the surface of the solid causing the liquid to bead up due to greater internal forces of the liquid compared to the surface [8]. Due to the inability to form bonds, the surface free energy is lower than that compared to other polymers.

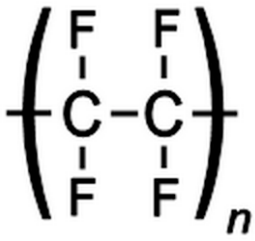


Figure 1 : The chemical structure of PTFE

2.1.2 Surface Roughness

Surface free energy is one of the governing factors in the wettability of the surface; however, surface morphology has shown to also contribute a significant effect [5]. The low surface free energy produced from compounds such as fluorocarbons see in Teflon can only obtain a maximum contact angle measurement of 100°, when wetted to water. To increase the contact angle the surface topography must posses a hierarchical micro-nano structure [10]. Introducing peaks and valleys in the surface paired with a hydrhophobic surface would cause the polar liquids to travel to the highest points to reduce contact with the surface to relieve surface tension [5]. As described in Equation 1, the surface free energy can be expressed with Young's equation; however, by incorporating the surface morphology, a surface roughness must be taken into consideration along with the contact angle. This may be described by Wenzel and Cassie-Baxter models that treat the combination of adding roughness to a wettable and non-wettable surface.

The Wenzel model, figure 2, shows that when a liquid interacts with the rough surface of a solid, the liquid will spread much faster to cover more surface area on a rough surface as a result of a greater net energy [5].

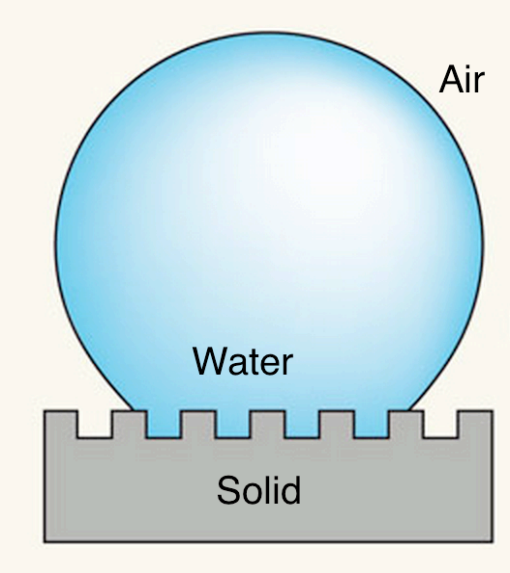


Figure 2: The Wenzel Model [11]

Equation 8 shows the addition of the roughness parameter to the surface free energy of the solid. The combination of the surface free energy described by Young's equation (Eq. 1) on a smooth surface along with a roughness parameter presents in Equation 8 results in Wenzel model shown in Equation 9.

$$\gamma_{lv}\cos\theta_w = r\left(\gamma_{sv} - \gamma_{sl}\right) \tag{8}$$

$$\cos\theta_w = r\cos\theta \tag{9}$$

where θ_w is the apparent contact angle measured from Wenzel's model, θ is the contact angle obtained from Young's equation, γ_{lv}, γ_{sv}, and γ_{sl} is the different interfacial tension between liquid, vapor, and solid and r is the surface roughness factor [5]. The roughness factor (r) can be obtained by measuring the actual surface and dividing it by the geometric surface. This model is typically used to describe hydrophilic or superhydrophilic surfaces.

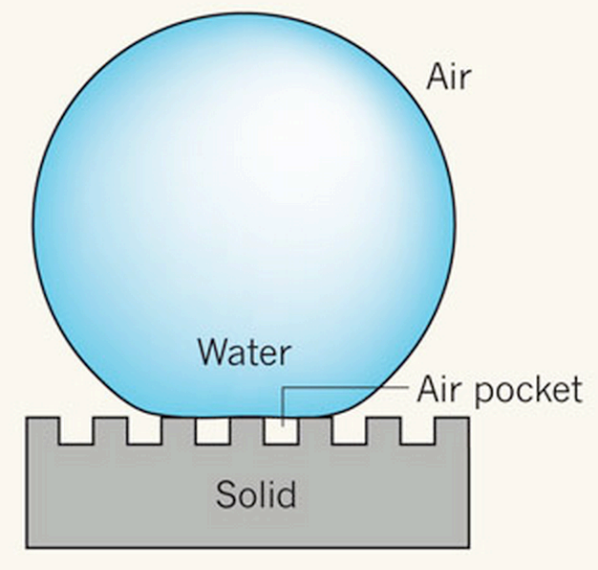


Figure 3: The Cassie-Baxter Model [11]

The Cassie-Baxter model (figure 3) is derived from the Wenzel model, but is applied for a surface with two interfaces (solid-gas and solid and liquid) as oppose to the one interface (solid-liquid). This model describes the response of a rough surface paired with a low surface free energy. Rather than liquid filling the pores of the surface, the liquid will be suspended on the high points of the surface introducing trap pockets of air in the structure [4]. This effect can be related to the contact angle on the surface that has fractal structures to produce Equation 10

$$\cos\theta_c = -1 + f_s\left(\frac{L}{l}\right)^{D-2}\left(\cos\theta + 1\right) \qquad (10)$$

where θ_c is the contact angel measured on a Cassie-Baxter model, f_s is the area fraction of the solid, L and l are the upper and lower limits of fractional behavior indicating the limits of the area fraction of the solid, and D is the fractal dimension [12]. This model is typically used to describe the behavior seen in superhydrophobic surfaces.

2.2 Superhydrophobic Surfaces

2.2.1 Natural Superhydrophobic Surfaces

The superhydrophobic property was first observed in nature in plants and insects. The lotus effect is commonly referred to the superhydrophobic effect seen in plants that results in self-cleaning of the lotus leaf [13]. This effect has not only been seen in the lotus plants, but in various other species of plants, all of which share common aspects that is results in this effect. This superhydrophobic effect is common in plants for self-cleaning purposes. Plant leaves are commonly exposed to particulates that often could cling to the surface of these leaves and germinate and cause damage to the plant [14]. When water is exposed to the surface of these plant leaves, assuming that the adhesion strength between water and the particulates are greater than that between the surface and the particulate, it will adhere to the water and be cleaned off the surface through natural forces such as gravity [14].

The construction of synthetic superhydrophobic surfaces are often inspired by the effect seen in nature such as in plants and insect. Through countless plant studies, it is seen that the surfaces of most plant leaves are composed of structural elements that contributes to the roughness of the surface [14-16]. These structural elements include trichomes and epicuticular waxes with the epicuticular relief range typically seen to be 5μm to 100μm and trichomes exhibits a maximum height of 2mm and is densely scattered over the surface of the plant [14]. These structural elements appears to assist in obtaining a superhydrophobic coating; however, without the addition of a nanostructured layer on the surface, it appear to have little to no effect on the superhydrophobicity of the leaf. The significant component seen in plants that does contribute to the superhydrophobic effect is the nanosized waxy crystallites seen at the ends of these structural elements. These waxy crystallites have been shown to be quite fragile and thus the environments with harsh rainfalls can cause abrasion on the surface of the leaf can removing the crystallites. This would then eliminating the superhydrophobic effect [14]. In the lotus leaf the epidermal cells produces a micrometer papilla that has nano-sized waxes layered on top seen in figure 4 [10]. The combination of the structural elements and these nanosized waxy crystallites indicates that to achieve a similar superhydrophobic structure seen in plant a hierarchical micro-nanostructure surface is necessary. This superhydrophobic surface seen in nature is designed

to assist plants in the removal of particulates and other various harmful substances that could affect the plant.

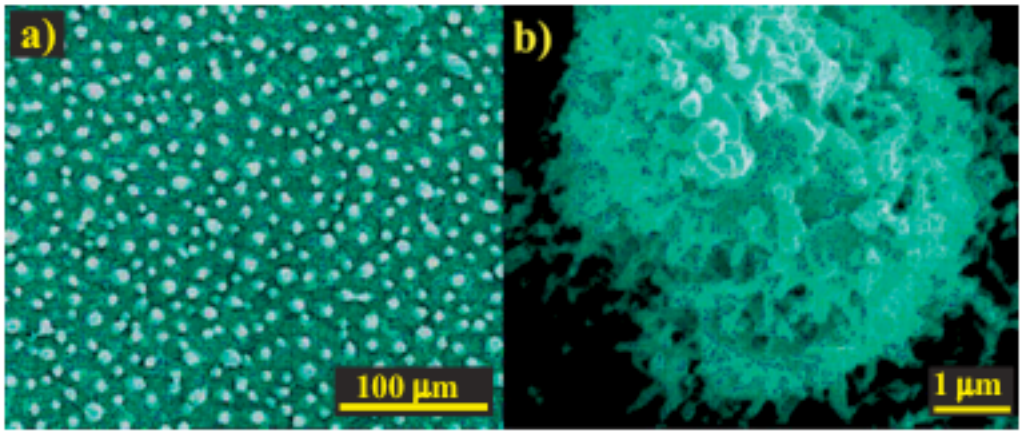


Figure 4: SEM images of the Lotus Leaf [10].

In addition to plants having natural superhydrophobic surfaces for self- cleaning aspects, various components of insects have also shown to have a superhydrophobic effect such as the wings of butterflies and moths[16-18]. When looking at the SEM images of the surface of large wings of insects such as dragonflies, it is shown to have a terry cloth-like microsculpture on the epicuticle cell that are approximately 0.3-0.5µm apart (figure 5) [19]. Water striders are an insect that has been seen standing or gliding on water and that ability is due to the superhydrophobic property seen in the legs. In figure 6, the leg is shown to be covered with tiny needle like hair known as microseta that contains nanogrooves building that desired hierarchical structure[17]. The wings of cicadae's also exhibits superhydrophobic properties that exhibits a slightly different structure then that seen in the legs of the water strider. The wings revealed to be composed of 70nm nanocolumns that are distant 90nm apart seen in figure 7 [18].

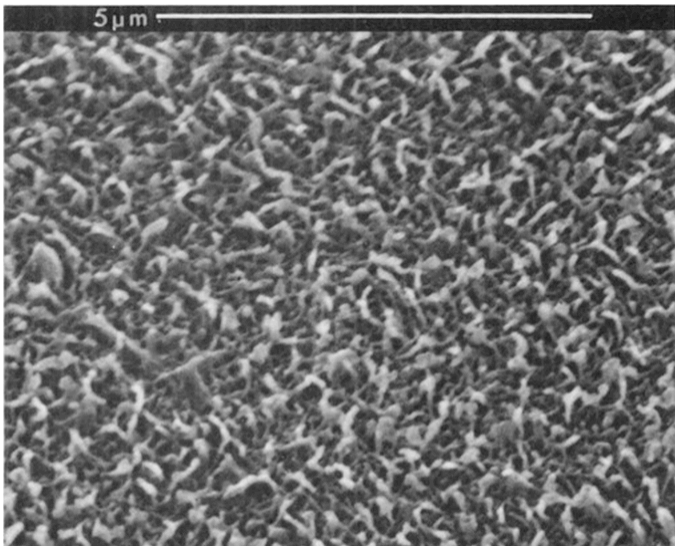


Figure 5: SEM images of *Planipennia* a species of insect with lace wings similar to that of mayflies and dragonflies [19]

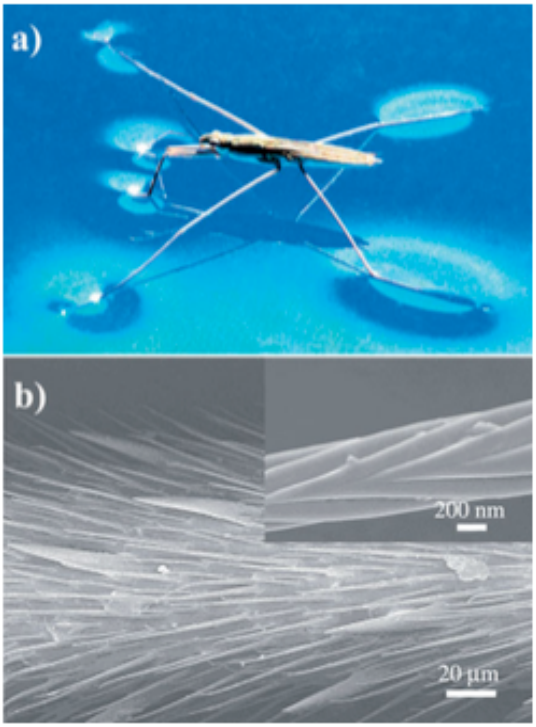


Figure 6: The SEM image of the superhydrophobic legs of *Gerris remigis* commonly known as water sliders [17].

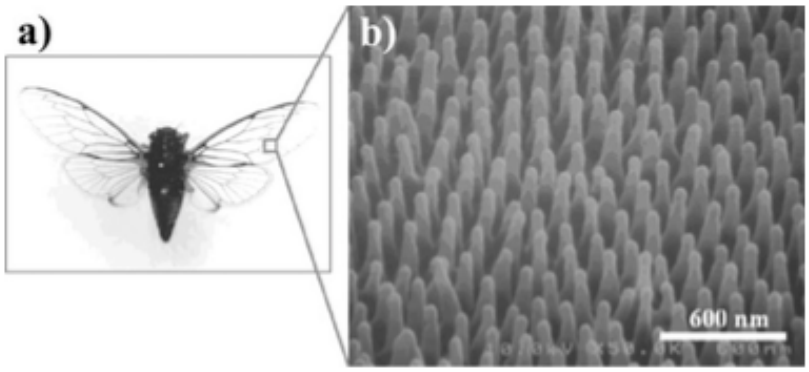


Figure 7: The SEM image of the superhydrophobic wings of *Cicada orni* commonly referred to as cicades[18].

2.2.2 Artificial Superhydrophobic Surfaces

The superhydrophobic surfaces seen in nature have proven to have two components: low surface free energy and rough surface topography. The Cassie-Baxter model combines these two components to describe the behavior of superhydrophobic surfaces. Several different methods have been developed to mimic the effect seen on the surface of plants and insect to develop artificial superhydrophobic surfaces. A low surface free energy can be obtained through materials that already exhibit this property or surface modifications can be utilized to create such a superhydrophobic surface by introducing functional groups such as fluorine or methyl. In addition to the low surface free energy, a rough micro-nano hierarchical structure must be created, which has can be achieved through methods such as template synthesis, layer by layer deposition, or phase separation.

2.2.2.1 Template Synthesis and Lithography

Template synthesis is a method used to imprint roughness onto the surface of the substrate. Nanosphere lithography is a common method that uses polystyrene (PS) and silica spheres templates to obtaining a patterned array of nanopores in large area [20, 21]. A film is deposited onto the template and after removal, the imprint of the pores remain intact. The roles can also be reversed to obtain a rough surface by having a self assembled particles rather than the removing the particles [22]. Chemical vapor deposition also utilizes templates to obtain appropriate surface morphology. In this case, the morphology of the

surface is dependent on the template. Chemical vapor deposition is a process that deposits reactive groups in gaseous form to react with the surface of the substrate to form a nonvolatile solid film [23]. This process has been used for preparing superhydrophobic textiles fabrics by growing polymethylsilsesquioxane nanofilments onto the fibers through a one step gas process [24]. The modified material exhibit long-term resistance to water during immersion and good abrasion resistances. Teshima et al. [25] use plasma etching on poly(ethylene terephthalate) (PET) substrates to create the morphology on the surface and plasma-enhanced chemical vapor deposition to functionalize the surface using tetramethylsilane (TMS). This process has shown to be convenient creating a superhydrhophobic surface through one step; however, the process is quite hazardous and requires expensive equipment.

2.2.2.2 Layer by Layer Deposition

The previous mentioned methods utilize the strategies to etch away areas to obtain nano-textured surfaces. Another approach to obtain these surfaces is rather than etching away material, one can build on the substrate to obtain the required rough morphology using methods such as layer-by-layer (LBL). LBL is a simple method used to develop these surfaces due to the large amount of control an individual on the thickness and properties of the coating [26]. This method is commonly used to fabricate multilayer polyelectrolytes through ionic assembly and can be applied towards constructing a thin film with nano-texture and low surface free energy as shown in figure 8 [27]. The ionic bonds used to assemble the surface are not as applicable for superhydrophobic applications due to the weak interactions. The stability of a superhydrophobic coating created by the LBL method is dependent on creating covalent bonds formed between each layer and to achieve this it is important to determine the proper chemical reactions performed in each layer. As mentioned a superhydrophobic surface is composed of a rough nano-textured surface and a low surface free energy, using the LBL deposition method functionalized nanoparticles are layered to form the desired rough surface [28]. In the final layer for the outer surface will typically contain reactive groups that will form covalent bonds with low surface free energy functional groups. This method has been expanded to be performed using various combinations of silica nanoparticles in epoxy-amino systems on organic/inorganic surfaces [29].The superhydrophobic surfaces obtained from the LBL method has been proven have a high contact angle measurements that scales with the amount of nanoparticle layers placed on the substrate, and great

durability due to the covalent bonds formed between each layer. However, this method can only be applied to smaller substrates and is quite expensive as well.

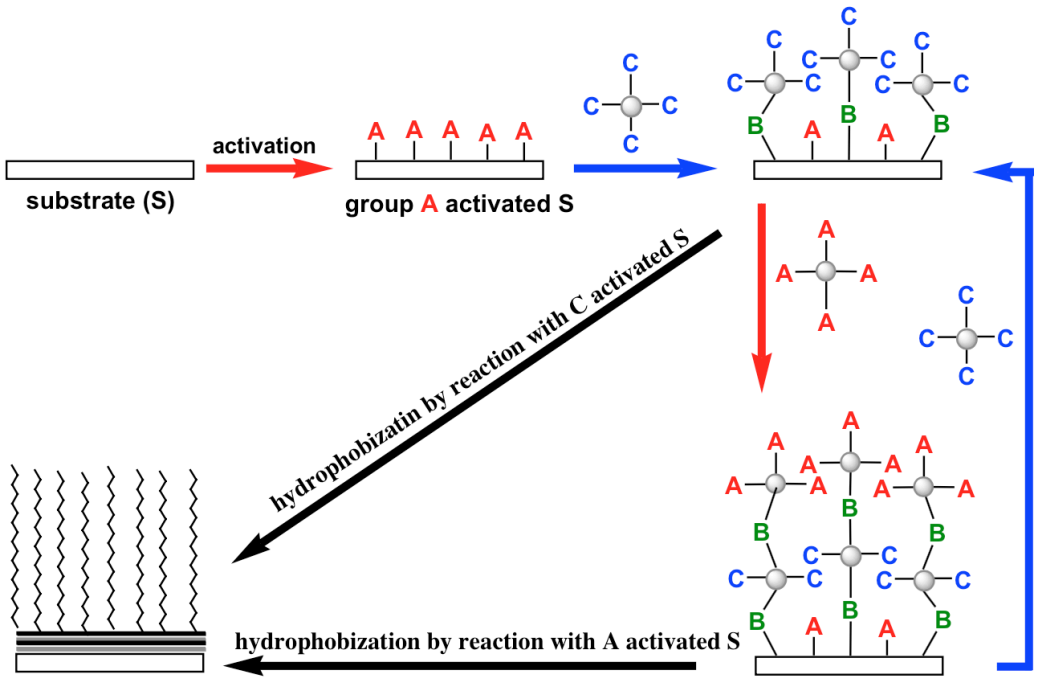


Figure 8: LbL method for producing superhydrophobic surfaces by applying nanoparticles with functional groups (A and C) are layered on top of the substrate and combined to form B functional groups that covalently joins the layers [30].

2.2.2.3 Phase Separation

Phase separation can also be used to fabricate porous materials through a hardening process that will be composed of a solid phase and a secondary phase, whether it be liquid or solid, that is removed to form a roughen surface [31, 32]. This process utilizes block copolymers that can from micelle in their respective solvent (figure 9). This is largely dependent on the concentration of the copolymer [33]. In large concentrations, the multimolecular micelles are formed which typically has a diameter ranging from 50 to 200 nm. The block copolymer is dissolved in a solvent, which will from a micelle solution. This solution is casted onto a substrate in which the solvent will evaporate revealing a roughen surface similar to that of the lotus leaf [33].

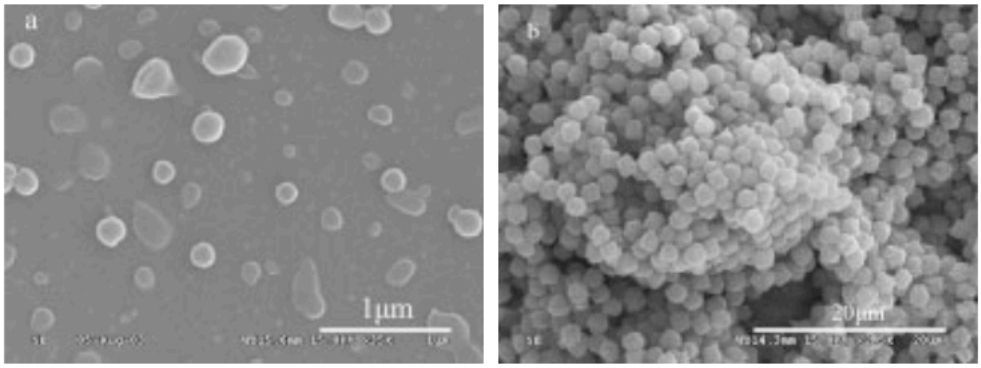


Figure 9: SEM images of PP-PMMA in a DMF solution a) with a concentration of $1x10^{-4}$ g m L^{-1} and b) with a concentration of $5x10^{-4}$ g m L^{-1} [33]

Another method of utilizing phase separation to create superhydrophobic surfaces was reported by Levkin et al.[34]. They polymerize common monomers in an inert solvent that results in phase separation that replicates the hierarchal micro-nanoscale roughness seen in nature. The cross-linked polymer chain obtained from this polymerization will reach a critical size will from a highly porous structure that is composed of interconnected globules (figure 10) This method is relatively simple and efficient and can be applied to large-scale surfaces; however, the durability of the coating is quite low and is quite dependent on the polymer film interaction to the substrate.

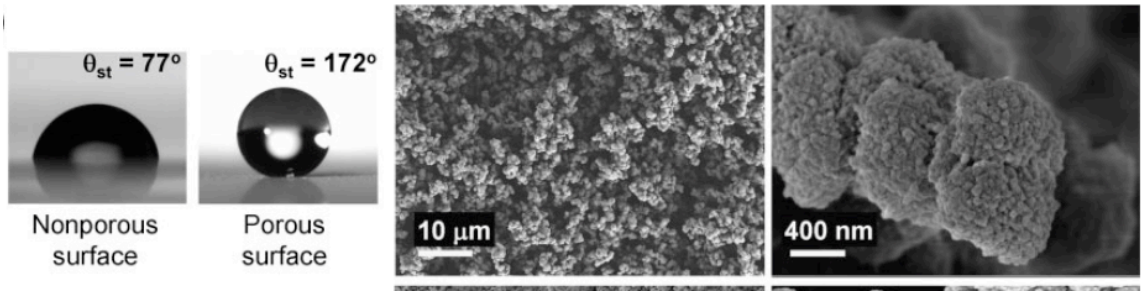


Figure 10: The difference in contact angle measured of a poly(butyl methacrylate-co-ethylene dimethacrylate nonporous and porous along with the SEM images of a superhydrophobic porous polymer [34]

2.3.1 Properties and Applications

There are a wide variety of applications that can utilize superhydrophobic surfaces. The most widely used application for superhydrophobic surfaces is for self-cleaning applications for glass windows especially skyscrapers although success is yet to be determined[35, 36]. This self-cleaning effect can also be applied towards architectural components such as roof tiles or incorporated into sprays and paints to obtain cleaner walls. Another huge market for superhydrophobic products is in the textile industry. The textile industry shows significant benefits to having a fabric that is water resistant while still keeping the fabric breathable and durable [24]. The fabric can also exemplifies self-cleaning properties. Water-resistance coating can be further expanded to other items such as umbrellas or awnings. Superhydrophobic coating can also be used for anti-biofouling applications. Biofouling is a huge problem seen in underwater structures and devices and often requires an exceptional amount of maintenance [37, 38]. A superhydrophobic surface will create a non-wettable surface that reduces the ability of microorganisms to attach; however, due to the harsh environment and long exposure can diminish the effect of the coating over time [39, 40]. Other industry applications for superhydrophobic coatings also include: anti-icing and anti-corrosion coatings [41, 42].

2.3 Polycarbonate (PC)

2.3.1 Introduction to Polymers

Polymers are a material class that is synthesized by a monomer to monomer link to form a molecular chain [43]. The joining of the monomer units is through a process known as polymerization that is caused by active centers known (anions, cation, and free radicals). A large portion of polymers is composed of hydrocarbon with covalent bonds that acts as the backbone of the polymer chain and the addition of other molecules will change the structure that could alter the properties and processing of the polymer as shown in figure 11.

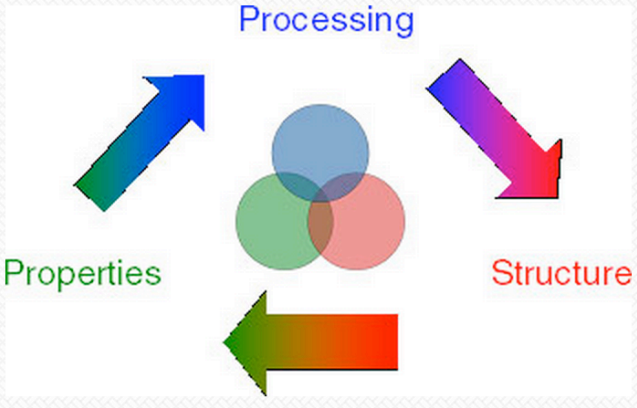


Figure 11: The relationship between structure, properties, and processing

There are two classes of polymers, natural polymers and synthetic polymers. Natural polymers are seen in nature such as cellulose, starch, and protein that are key components in the biological and physiological aspects of plants and animals [43].The discoveries of these natural polymers then lead to the development of synthetic polymers such as Polyethylene (PE) and Polycarbonate (PC) that can be used for a wide variety of applications. The advantages of synthetic polymers are the wide range diversity of polymers that exhibits different properties such as corrosion resistant, impact resistant, elasticity etc. Synthetic polymers are also an inexpensive material to process and obtain.

The molecular weight (M_w) is an important component that is related to the length of the chain. Since the chains in a polymer are produced at various lengths during polymerization, the Mw is often measured as a distribution. The Mw has an essential role in the properties seen in the polymer such as the melting temperature of polymers. An increase in the Mw will also cause an increase in the melting temperature of the polymer. There are also correlations between the Mw and the elastic modulus and strength of the polymer [43]. The various lengths and chains in a polymer introduces a molecular shape that has been known to effect the mechanical and thermal properties of the polymer and this is seen due to the rotation and flexibility of the chains. Polymers can also be classified due to their behavior at high temperatures. Thermoplastic polymers has a tendency to soften with heat and this due to the breaking of the secondary bond and melting of crystals by the increase in molecular motion [43]. Thermoset polymers are able to withstand high temperatures and are often seen in network polymers that are cross-linked with covalent bonds.

Polycarbonate (PC) is an amorphous thermoplastic polymer that offers a wide variety of properties that can be used for various applications due to its optical transparent properties and reasonable mechanical properties. The name polycarbonate is related to the carbonate groups (C=O) found in the structure of the monomer (figure 12). PC can be obtained through an interfacial polycondensation reaction using 2,2-bis(4-hydroxylphenyl)propane, commonly known as bisphenol A (BPA), as the monomer or it can be obtained through melt transesterification.

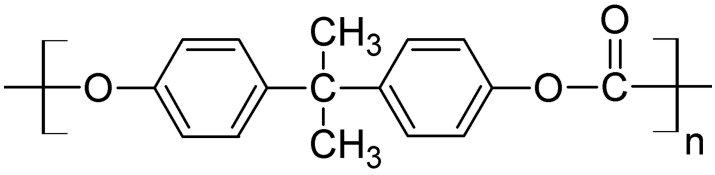


Figure 12: Polycarbonate chemical structure

2.3.2 Properties and Applications

Polycarbonate (PC) is best known for its properties (table 1) that include high toughness and heat resistances paired with the optical transparency. Another property that is unique to PC is its compatibility with other polymers to form blends to alter and improve its properties [44]. The most widely used polycarbonate is BPA-PC. BPA-PC is used for a variety of applications such as electrical sector, building and construction, and automobiles. PC has shown to be used in a variety of electrical components in modern day applications such as housing for various electronic materials, lamp sockets, and power plugs. It is an ideal polymer to use for these applications due to its toughness and heat resistances, as mentioned above, as well as its excellent electrical insulation [45]. In addition to the great properties of PC, it is also quite inexpensive which makes it a cost effective material for the construction industry. The optical transparent quality and high impact resistance of PC allows it be used as windowpanes and roofing for various locations [45]. PC is also commonly used as headlights and taillight covers in the automotive industry and a PC/ABS blend is used for dashboard of cars. This polymer can also be put into solutions to form films on variety of substrates while still maintaining its properties.

Table 1: BPA-PC properties using various testing standard [44]

Property	Test Standard	Value
Tensile modulus, MPa	ISO 527-1,-2	2400
Yield stress, MPa	ISO 527-1,-2	66
Yield strain, %	ISO 527-1,-2	6.2
Stress at break, MPa	ISO 527-1,-2	70
Norminal strain at break, %	ISO 527-1,-2	> 50
Impact strength at 23°C, kJ/m^2	ISO 179-1eU	Unbroken
Impact strength at -30°C, kJ/m^2	ISO 179-1eU	Unbroken
Notched Impact Strength at 23°C, kJ/m^2	Based on ISO 179-1eA	75
Notched Impact Strength at 23°C, kJ/m^2	Based on ISO 179-1eA	16
Ball indentation hardness, N/mm^2	ISO 2039-1	115
Vicat softening temperature (50N; 120°C/h), °C	ISO 306	146
Temperature of deflection under loat (1.8 MPa), °C	ISO 75-1,-2	125
Coefficient of linear thermal expansion, K^{-1}	ISO 11359-1,-2	6.5×10^{-5}
Thermal conductivity (23°C; 50% R.H), W m^{-1} K^{-1}	ISO 8302	0.2
Burning behavior at 0.75 mm	UL 94	Class V-2
Glow-wire flammability test (GWFI) at 0.75mm, °C	IEC 60695-2-12	850
Oxygen index (method A) in %	ISO 4589-2	28
Relative permittivity (100 Hz/1MHz)	IEC 60250	3.1/3.0
Dissipation factor (100 Hz/MHz)	IEC 60250	5×10^{-4} / 90 x
Volume resistivity, Ω m	IEC 60293	10^{-4}
Surface resistivity, Ω	IEC 60293	10^{14}
Electrical strength at 1mm, kV/mm	IEC 60243-1	10^{16}
Moisture absorption (23°C, 50% RH), %	Analogous to DIN 53 495-1	34
Refractive Index (Procedure A)	L	0.15
Luminous transmittance (clear transparent materials) at 1mm, %	ISO 489 ISO 13468-2	1.586 89
Density, kg/m^3	ISO 1183-1	1200

2.3.4 Polycarbonate Degradation

Polymers are used for a variety of applications that involves exposure to environmental factors such as UV, moisture, and temperature fluctuations. These factors have been proven to cause degradation in the polymer decreasing its properties and performance. In several studies [46], PC has shown that exposure of UV radiation can diminish the transparent properties by causing a discoloration and haze to appear on the surface of the polymer. Humidity has also been seen to degrade PC by causing hydrolysis in the polymer creating a chemical breakdown [46]. The thermal exposure to PC initiates chemical reactions that cause molecular chain degradation. The reactions responsible for the degradation of PC are photo-Fries reaction and photo-oxidation reactions [47]. Photo-fries reactions in figure13 is initiated through the producing of free radicals in the structure caused by the scission of the carbonate bonds [47]. The free radicals will cause cross linkages to form and rearrangement in the polymer

chain to form various molecules that eventually lead to production of substances such as diphenoquinone and ortho-diydroy-benzophenone that are responsible for the yellowing of the PC under UV exposure [47].

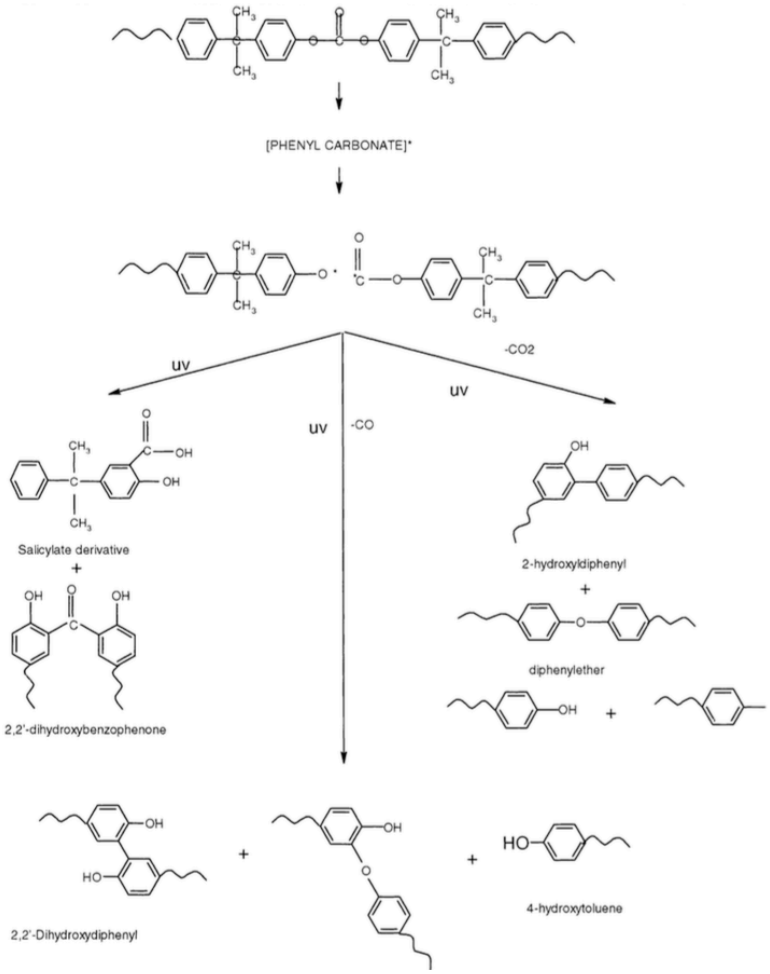


Figure 13: Photo-Fries Mechanism [48]

Photo-oxidation mechanism shown in figure 14 is another reaction scheme responsible for the degradation of PC [47]. There are three ways that this reaction can target the PC: side chain oxidation ring oxidation and ring attack. Although each one has a contributing effect to the degradation of this polymer, the most common is the side chain attack reaction which is due to the energy absorbed by UV radiation that forms free radicals from methyl groups. When oxygen is introduced into the reaction it produced hydroperoxide intermediates that can terminate or prolong the reaction. This reaction is seen to be more prominent on the ends of the polymer chain causing the reduction in molecular

weight. It has been proven that the more prominent reaction is the photo-oxidation mechanism, nevertheless, both are active during the degradation process [47].

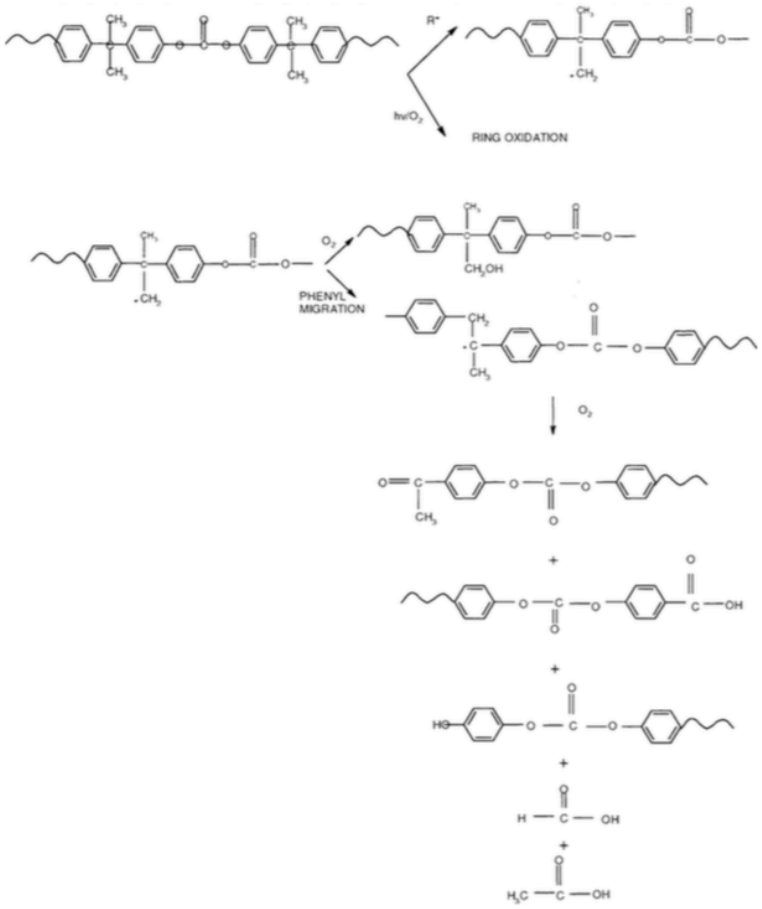


Figure 14: Photo- Oxidation Mechanism of PC [48].

2.4 Transparency and Optics

Optical transparency is the ability of light to transmit through a material without significant scattering or absorption. As mentioned, superhydrophobic surfaces are generally composed of micro-nano roughness components that correlate with the superhydrophobicity of the surface. This micro-nano roughness has the potential to act as scattering centers scattering light resulting in a non-transparent coating. To obtain a transparent superhydrophobic coating, the micro-nano roughness must be reduced to a nano-nano roughness. Optical

transparency is an important property that is essential for a variety of devices such as windows, camera lenses, and automobile taillights.

2.4.1 Introduction to Optics

The optical properties in a material is often related to the response of the material when exposed to electromagnetic radiation such as visible light [43]. Electromagnetic radiation can often be described as a wave that is composed of an electric and magnetic field. The electromagnetic spectrum of radiation (Figure 15) includes all forms of electromagnetic radiation (light, heat, x-rays etc.) and is used to characterize the different forms. The electromagnetic radiation wavelength of light ranges from 700nm to 400nm, which can be visualized by the naked eye.

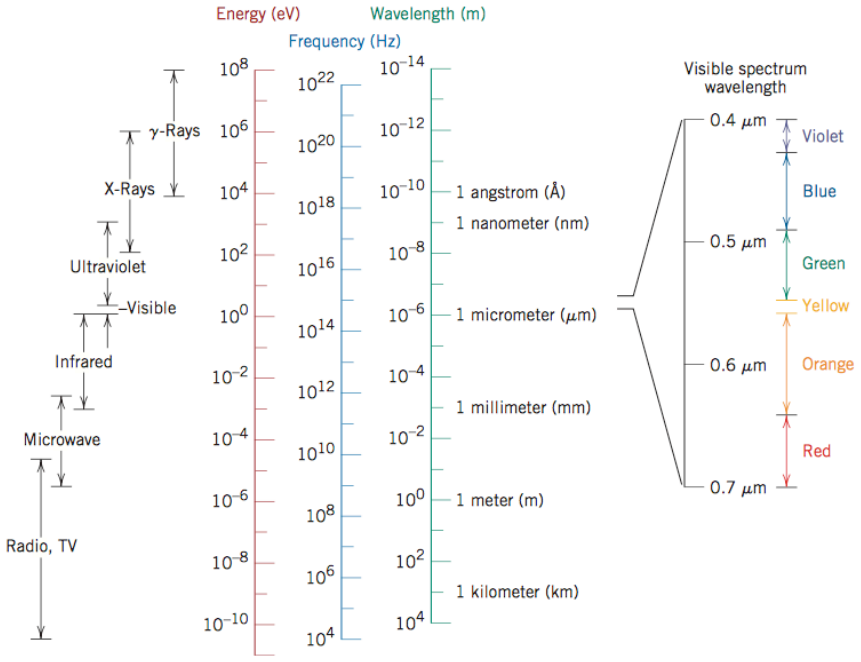


Figure 15: The Electromagnetic Spectrum [43].

When light interacts with a solid it can either be transmitted through, reflected at the interface or be absorbed. This can commonly be expressed by intensities in equation 11, where the sum of the intensities of the transmitted, reflected and absorbed must equal the intensity of the incident beam[43].

$$I_o = I_T + I_A + I_R \quad (11)$$

where I_0 is the incident beam and I_T, I_A, and I_R are the intensities of the transmitted, absorbed, and reflected. Materials that are unable to transmit visible light are referred to as opaque materials. The opaque quality of metals is different than that seen in dielectric materials. In metals the opaque appearance is due to the unoccupied energy states that are filled when the incident radiation excites electrons from the ground state. This results in an absorbance of the incident radiation that is then remitted as reflected light. In dielectric materials the cause of the opaque appearance is due to the transmitted light scattering extensively that results in no transmission of the incident beam.

2.4.2 Shell's law

Transparent materials have the possibility of transmitting, absorbing, and reflecting light. The velocity of light traveling in a vacuum will decease when entering another medium resulting in a bent interface referred to as refraction [43]. A common ratio used to measure the degree of bending that occurs is known as the index of refraction (equation 12)

$$n = \frac{c}{v} \quad (12)$$

where *c* is the velocity of light in a vacuum and *v* is the velocity of light in a medium. When the index of refraction is greater it indicates that the electronic polarization is greater and the velocity of light is slower presenting a less transparent material. The transmission of light through a transparent material can be described by Snell's Law in figure 16 and is governed by equation 13

$$n_1 \sin\theta_1 = n_2 \sin\theta_2 \quad (13)$$

where n_1 and n_2 is the index of refraction of the two medias and θ_1 and θ_2 is the angle of the incident beam and refractive beam.

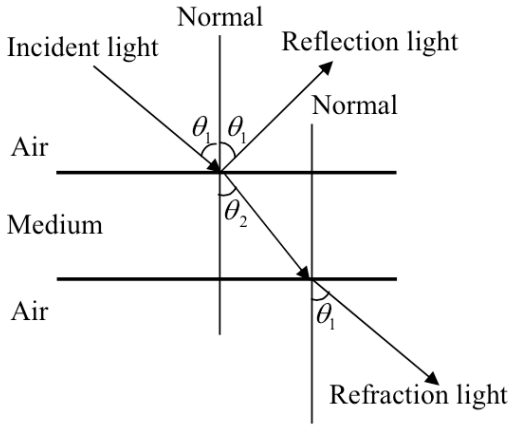


Figure 16: Shell's Law

Despite having a transparent surface, light will still reflect at the interface between two medias having different index of refraction. The reflectivity (*R*) of the incident light is dependent on the interaction of light on the interface. If light is normal to the interface the reflectivity will be represented using equation 14, and if it is not normal equation 15 will be used [43]

$$R = \left(\frac{n_2 - n_1}{n_2 + n_1} \right)^2 \qquad (14)$$

$$R = \left(\frac{n_s - 1}{n_s + 1} \right)^2 \qquad (15)$$

where n_2 and n_1 are the indices of refraction of the two medias and n_s is the index of refraction for the solid when light is transmitted from air to the solid. The index of refraction of the medium, which light penetrates when leaving air, is largely dependent on the reflectivity. The increase in the index of refraction will result in greater reflectivity. To allow for more transmission of light through the medium, an anti-reflective coating such as magnesium fluoride (Mg_2F_2) will often be added to the surface [43]. This type of coating causes the incident beam to act on a two-interface system that will be separated by a specific thickness to produce reflected beams from the coating and the medium that will result in destructive interference. This would result in less reflection from the medium and more transmission.

CHAPTER III
MATERIALS AND METHODS

3.1 Development of Coating

3.1.1 Materials

Pre-functionalized aerogel was purchased from Cabot (Boston, MA). Polycarbonate (PC) [Poly (bisphenol-A carbonate] (MW of 36,000) was purchased from Scientific Polymer Products, Inc. The solvent used was tetrahydrofuran (THF) purchased from Sigma Aldrich for dissolving the PC. The Retsch Ball Mill along with a 50ml Retsch ZrO_2 canister and ZrO_2 balls (8.6mm) were used to break down the aerogel particles. The ultrasonic probe was purchased from Vibra Cell used with the Sentry Air Systems Inc. portable hood snorkel. The Wrist Action Shaker (Burrell) was used to mix the PC in solution. Cleaning Chemicals included Acetone, Ethanol, Micro-90 concentrated cleaning solution for cleaning glassware used during the experiment, and DI water.

3.1.2 Preparation of coating solution

Pre-functionalized aerogel is placed in the 50ml $YZrO_2$ canister with tetrahydrofuran (THF) and ZrO_2 balls to form a 0.3wt% concentration. The solution is placed in the ball mill at a milling speed of 100rpms for 24 hours. The solution was milled at 1-minute intervals with a 30 second break. The milled aerogel solution is poured into a beaker and placed in an ice bath to prevent over heating during the ultrasonication process. The Ultrasonic probe is placed in the solution and used with a standard frequency between 20-10 Hz for 10 minutes to allow for sufficient time for the aerogel to break down to nano-sized particles. The volume sonicated aerogel solution is measured and mixed with PC to create a 0.1wt% concentration of PC and sonicated aerogel in THF resulting in a 3:1 ratio of aerogel to PC. This mixture is placed in the shaker for 30 minutes to guarantee the dissolution of the PC pellets.

3.1.3 Spin Coating

Using the Model WS-400 BZ-8TFM/LITE spin coater, a variety of substrates were coated including: 2” diameter silicon wafer and 1.1 x 1.8 “ quartz glass. Prior to coating, the substrate was cleaned with acetone and then methanol. The substrate was held onto the spin coater through a vacuum and approximately 2 ml of solution was dispersed onto the substrate. The substrate was spun at 2500rpms for 25 seconds and the process repeated with the deposition of more solution onto the substrate for an addition of 3-5 times depending on the desired

coating. A superhydrophobic polycarbonate coating (SHPC) was produced for one layer (SHPC 1X), three layers (SHPC 3X), five layers (SHPC 5X), and ten layers (SHPC 10X). The deposited films were air dried after spin coating and subjected to further characterization.

3.2 Characterization

3.2.1 Fourier Transform Infrared Spectroscopy (FTIR)

The PerkinElmer Spectrum One FT-IR spectrometer was used to collect the FTIR spectrum of the superhydrophobic polycarbonate coating coated ten times (SHPC 10X) on a silicon wafer for functional group analysis. Using a Type IIIA diamond attenuate total reflectance (ATR), at a 45° angle of incident, the transmission spectrum was obtained each was the result of a total of 16 scans from 4000 to 600 cm^{-1} wavenumbers.

3.2.2 Scanning Electron Microscope (SEM) and EDS

A Leo 1525 scanning electron microscope (SEM)® equipped with Zeiss SmartSEM Software was used to obtain micrographs of the surface of the coating. All surface micrographs were captured of using an accelerated voltage of 1 keV at various magnifications with the SE-2 detector. The micrographs of the thickness of the coating were also captured using an accelerated voltage of 1 keV at various magnifications but with an InLens detector instead. An additional x-ray detector was also attached to the SEM to perform elemental analysis using energy dispersive spectroscopy (EDS) at an accelerating voltage of 5keV.

3.2.3 Atomic Force Microscopy (AFM)

The XE-100 Advanced Scanning Probe Microscope AFM® is a technique used to obtain images of the surface topography of the coating. Compared the SEM, which uses high energies that could potential damage the surface of the coating, the AFM uses a Pointprobe –monolithic silicon–nanotip probe that has a tip radius of curvature of less than 8 nms. The AFM measurement was taken in non-contact mode, which measures the surface topography through oscillation at a resonant frequency 320 kHz.

3.2.4 Light Transmission

Transmission was measured using the Cary 5000 UV-Vis MR Spectrometer. The measurement was carried out through the wavelength of 800nm-200nm on the SHPC 1X, 3X, 5X, and 10X samples. The transmission spectra was the average of two runs. The transmissions of these coatings are then compared to transmission of quartz glass as a reference.

3.2.5 Contact Angle Measurement (CA)

Contact angle (CA) is a common measurement tool used to determine the superhydrophobicity of a surface and the surface free energy. The ChemInstrument Cam-Plus® was used to obtain the CA for films deposited on quartz substrates. The measurement utilizes a simple equipment that is consists of a protractor, a light source, and pipet. The SHPC samples are mounted to the stage of the instrument and aligned parallel to the protractor. A 25µl to 30µl droplet is placed on the surface of the sample with the light source projecting a shadow of the droplet onto the protractor, where the contact angle is measured. This measurement is performed at a line across the sample to obtain a better estimate of the CA of the coating. Five points were measured on each sample as shown in figure 17 for SHPC 1X, 3X, and 5X coating along with a non-coated quartz substrate.



Figure 17: Five points were measured for the CA for the SHPC coating

3.2.6 Nanoindentation

Using the Hysitron Indenter® with a Berkovich diamond tip, the SHPC 1X, 3X, 5X, and 10X coatings on silicon wafers substrate were measured. The measurement was used to obtain the hardness and modulus of the coating with different thicknesses. Twenty points were measured with a 300μN load with a 3 sec loading, a 10 sec hold, and then a 3 sec unloading cycle.

CHAPTER IV
RESULTS

5.1 Surface Chemistry and Topography

5.1.1 Elemental and Functional group analysis

The superhydrophobic polycarbonate coating (SHPC) is obtained with low surface free energy and rough surface topography. The initial intent is to create a surface that has low surface free energy by applying the appropriate functional groups to achieve this surface. The SHPC coating in this study is composed of functionalized aerogel nanoparticles embedded in a PC matrix. The elemental analysis of this coating is done using energy dispersive spectroscopy (EDS) and is further characterized to confirm functionalization of the coating by using fourier transform infrared spectroscopy with attenuated total reflectance (FTIR-ATR). Figure 18 and 19 shows the EDS spectrum obtained from a SHPC 1X and SHPC 10X coated silicon wafer. The measurement was obtained at a magnification of 3728X and 1863X with an accelerating voltage of 5kV. The EDS analysis of the SHPC 1X indicated the presences of C, O, and Si with an elemental composition of 8.14wt%, 4.60wt% and 87.26wt% (Appendix 1). This indicates that there is a presence of PC and aerogel with correlates with the 3:1 ratio for the coating. Another EDS spectrum was obtained for a SHPC 10X coating on a silicon wafer (figure 16) that exhibited same elements, but with a increase in the O concentration by 12wt% and a decrease in the Si concentration by 12wt%. The cause for the reduction in silica is due to the thickness of the coating and the x-ray beams depth of penetration. The depth of penetration is depended on the accelerating voltage and the density of the coating. The deeper the depth of penetration the more likely the substrate will be accounted for in the measurement, giving inaccurate results for the coating.

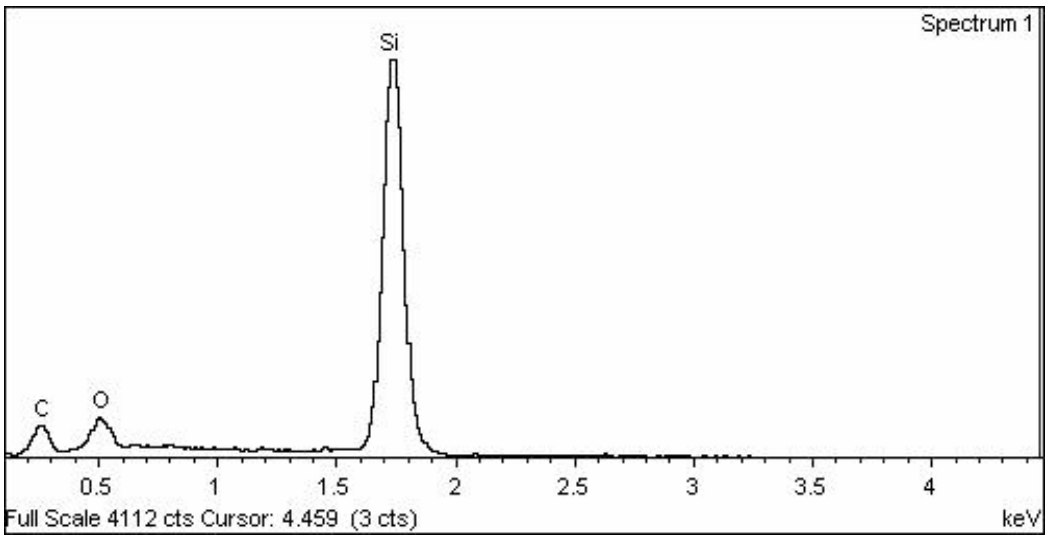


Figure 18: EDS spectrum of SHPC 1X coating on a silicon wafer at 1863X.

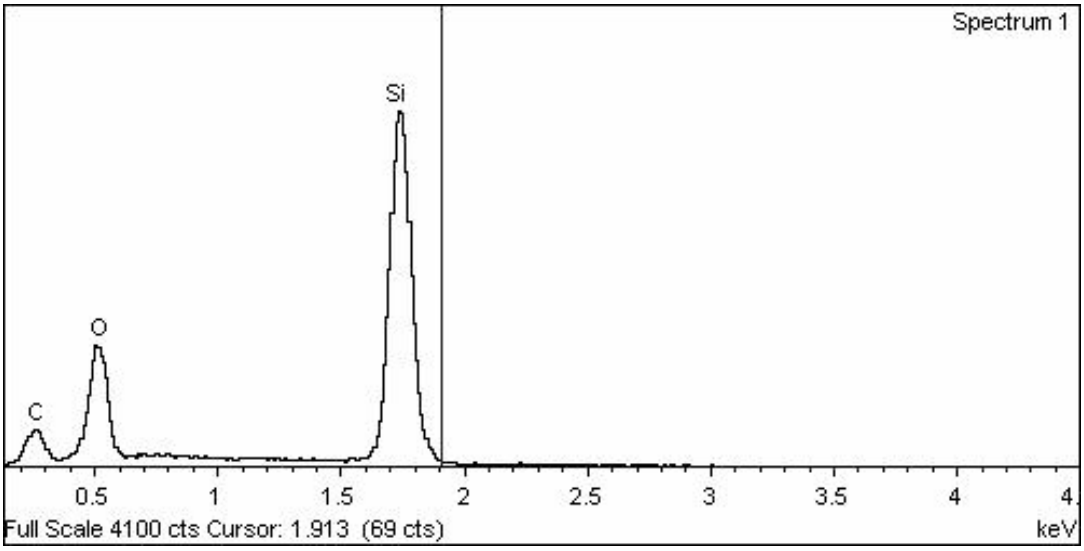


Figure 19: EDS spectrum of the SHPC 10X coating on a silicon wafer at 3728X.

The characterization of the surface composition was further analyzed using attenuated total reflectance (ATR) with the FTIR for functional group analysis. The FTIR spectrum of the SHPC 10X coated silicon wafer in figure 20 is measured in transmission at a total of 12 scans. The spectrum shows a distinct C-H stretching peak at 2966 cm^{-1} followed by a carbonyl C=O stretching peak at 1750 cm^{-1}, and a benzene ring breathing absorption band at 1509 cm^{-1} [49]. The

carbonyl stretch is typically seen at 1725 cm^{-1} and the benzene stretch at 1600 cm^{-1}, the shift down to lower wavenumbers could be due to the addition of the aerogel in the PC. These three characteristics peaks are expected to represent the composition of PC. The major peak occurring around 1100 cm^{-1} represents the Si-O peak, which represents the aerogel present in the coating an potential some of the silicon substrate. The doublet peak located at 1195 cm^{-1} and 1188 cm^{-1} represents the CF_2 symmetric stretching [49].

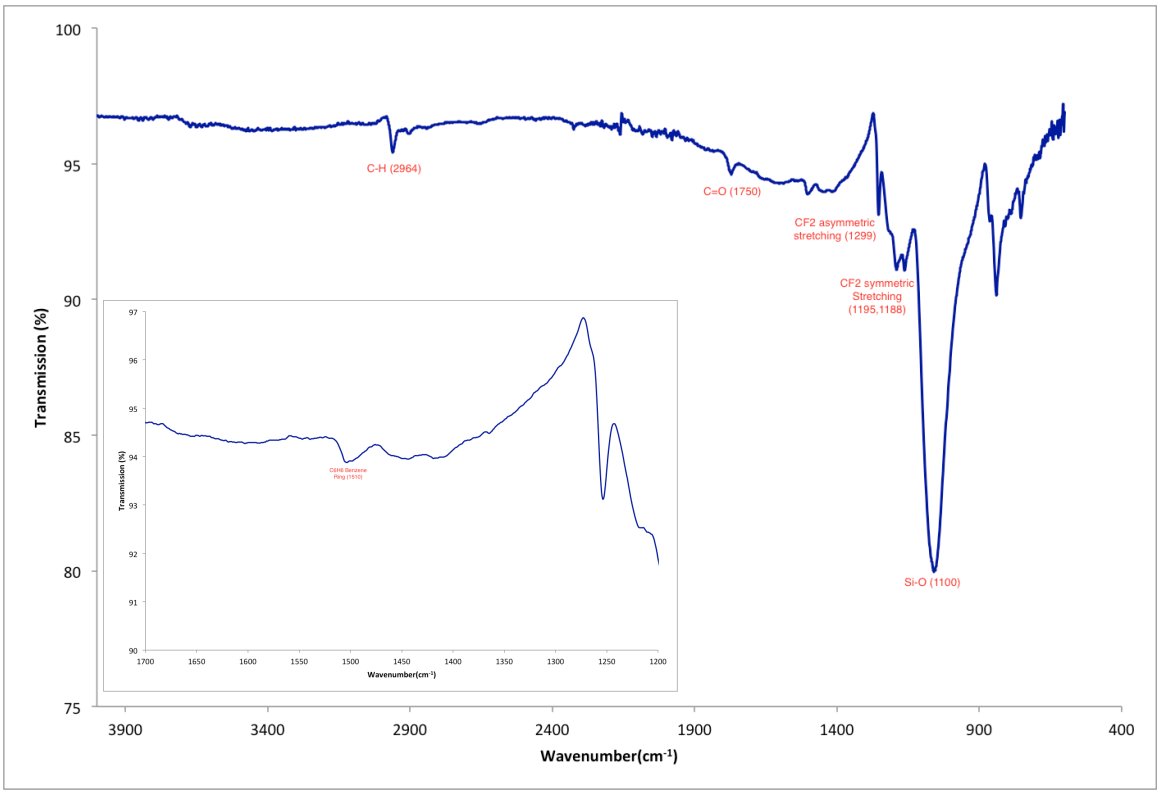


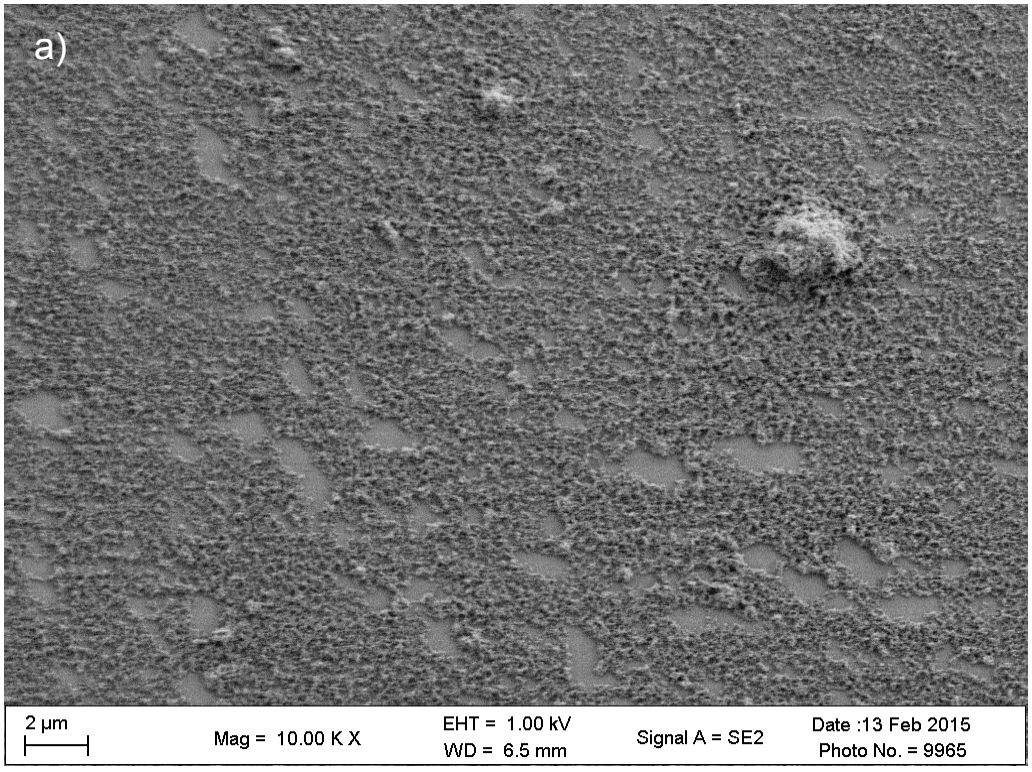
Figure 20: The FTIR spectrum of SHPC 10X coating on a silicon wafer using ATR.

5.1.2 Surface Micrographs (SEM)

An extensive study of the surface topography was initialized using the SEM. The surface topography and the distribution of the coating on the surface were obtained for a SHPC 1X, 3X, and 5X coating on a silicon wafer. The micrographs were obtained at a relatively low voltage of 1kV to prevent damaging and charging of the coating. The SHPC coating images are taken at 10KX, 25KX, and 100KX magnification. The micrographs indicated the coverage for different

coatings with the largest gap length ranging from 1.5μm to 360nm for the SHPC 1X coating (Figure 21). The gap length decrease significantly in the SHPC 3X coating from 790nm to 500nm (Figure 22), until there were no gaps present in the SHPC 5X coating (Figure 23).

Figure 21: The SEM micrographs of SHPC 1X coating on a silicon wafer at a) 10KX, b) 25KX, and c) 100KX with indication of coating distribution.



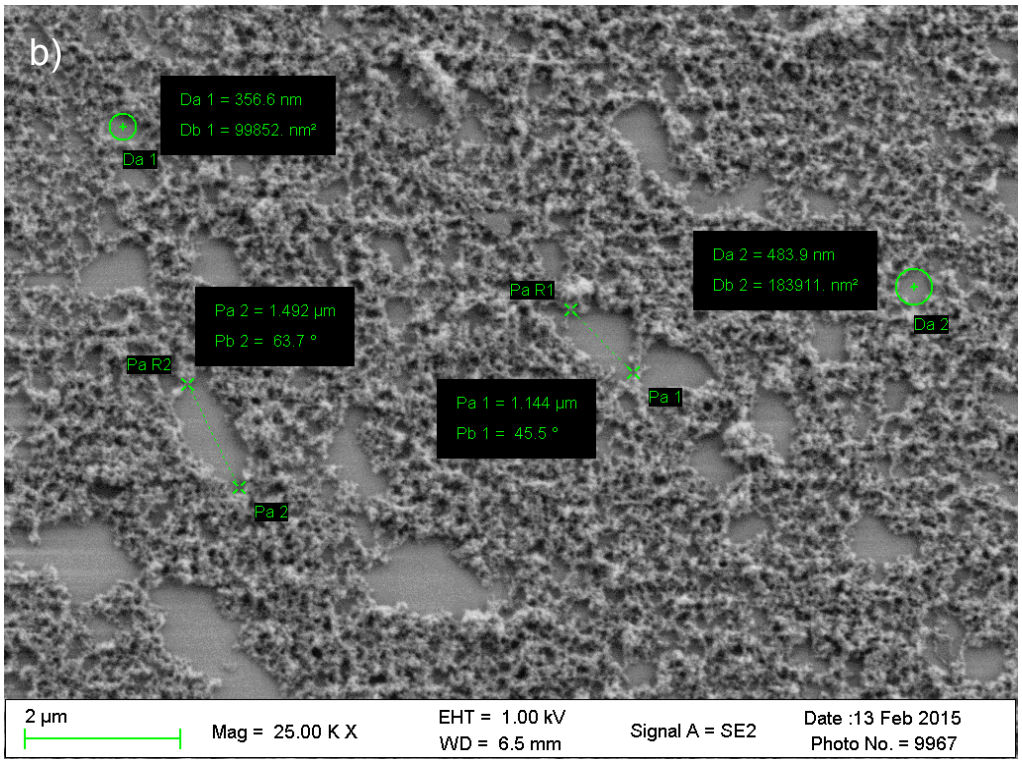


Figure 21 Continued

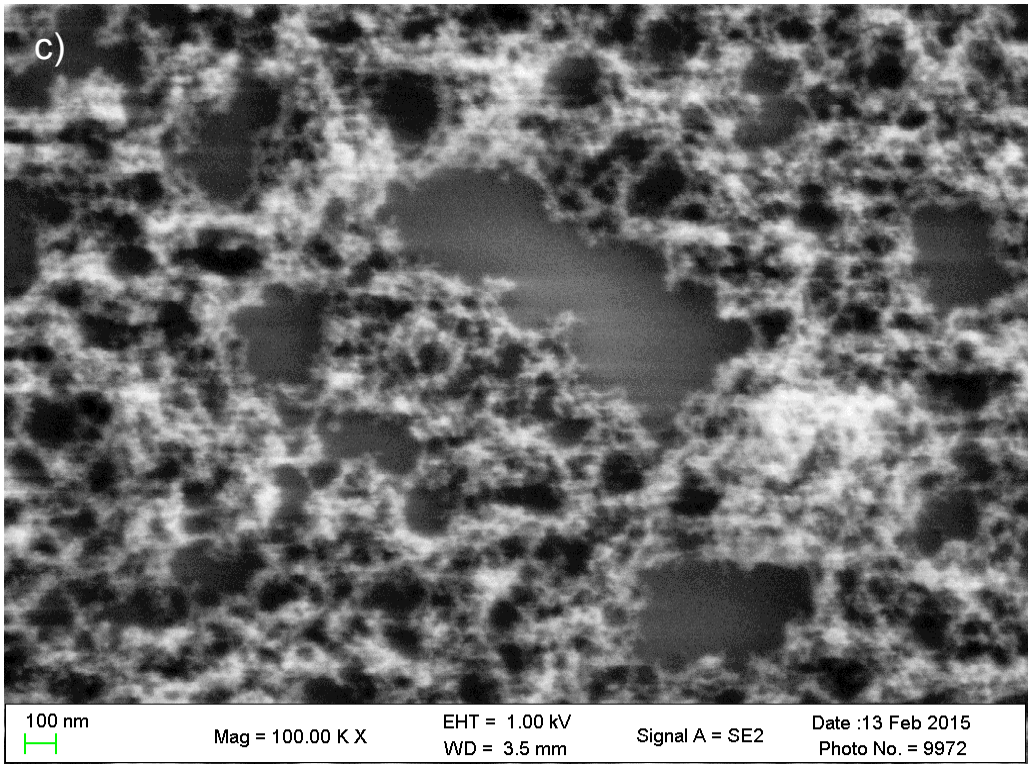
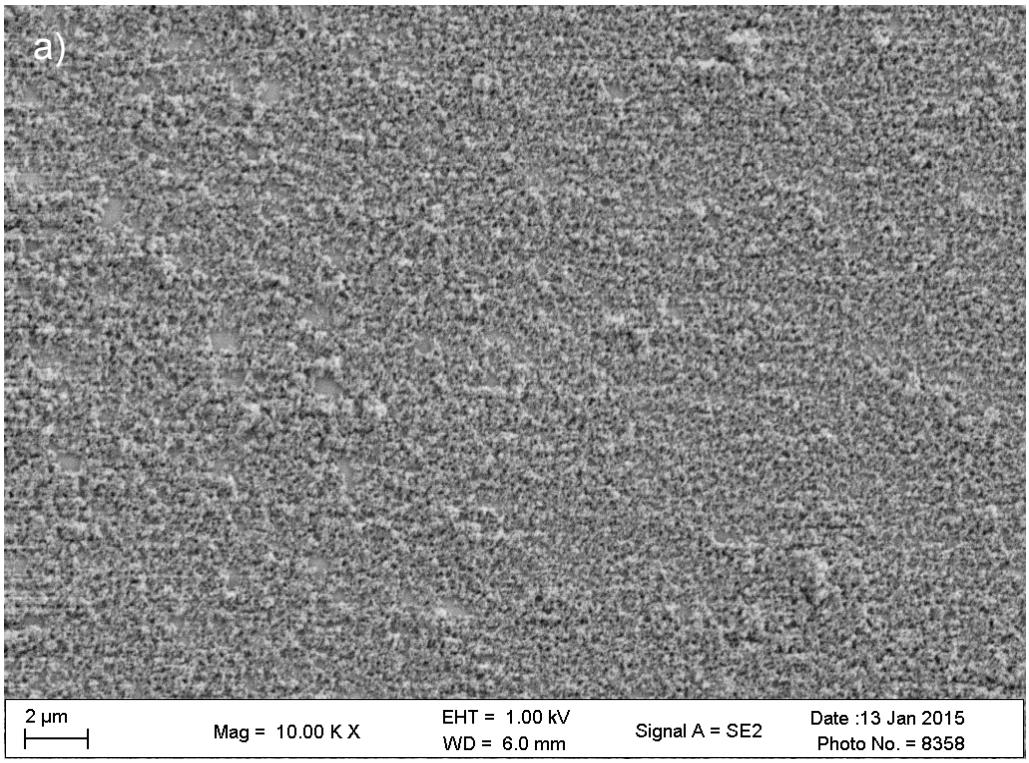


Figure 21 Continued

Figure 22: The SEM micrographs of SHPC 3X coating on a silicon wafer at a) 10KX, b) 25KX, and c) 100KX with indication of coating distributions



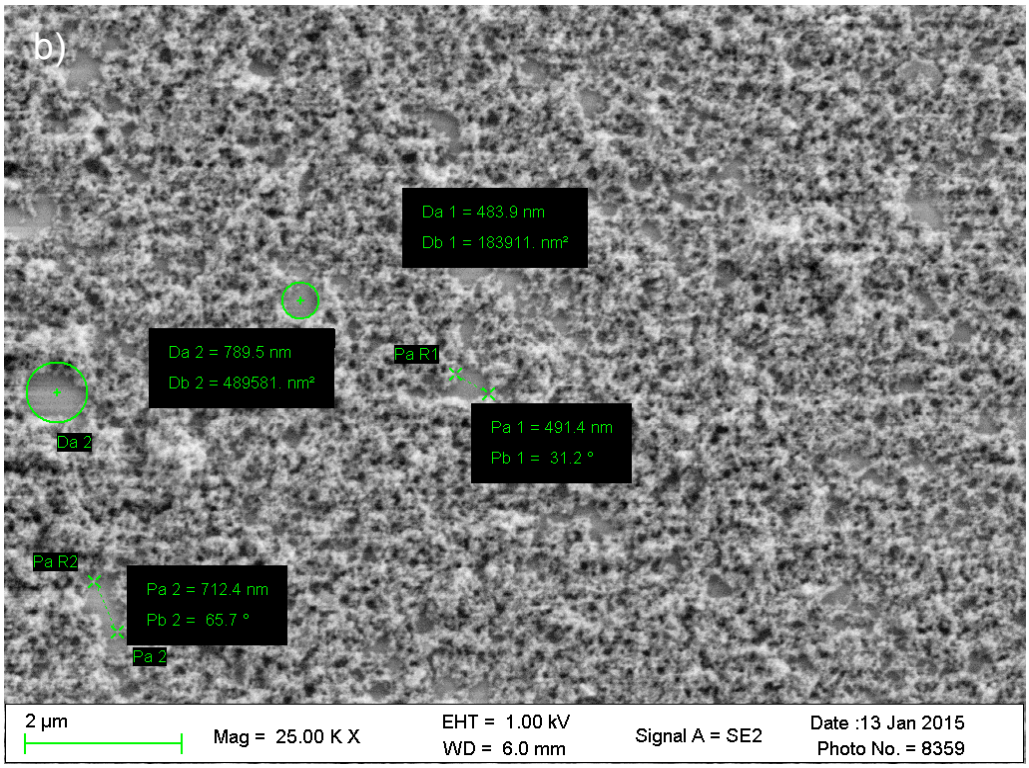


Figure 22 Continued

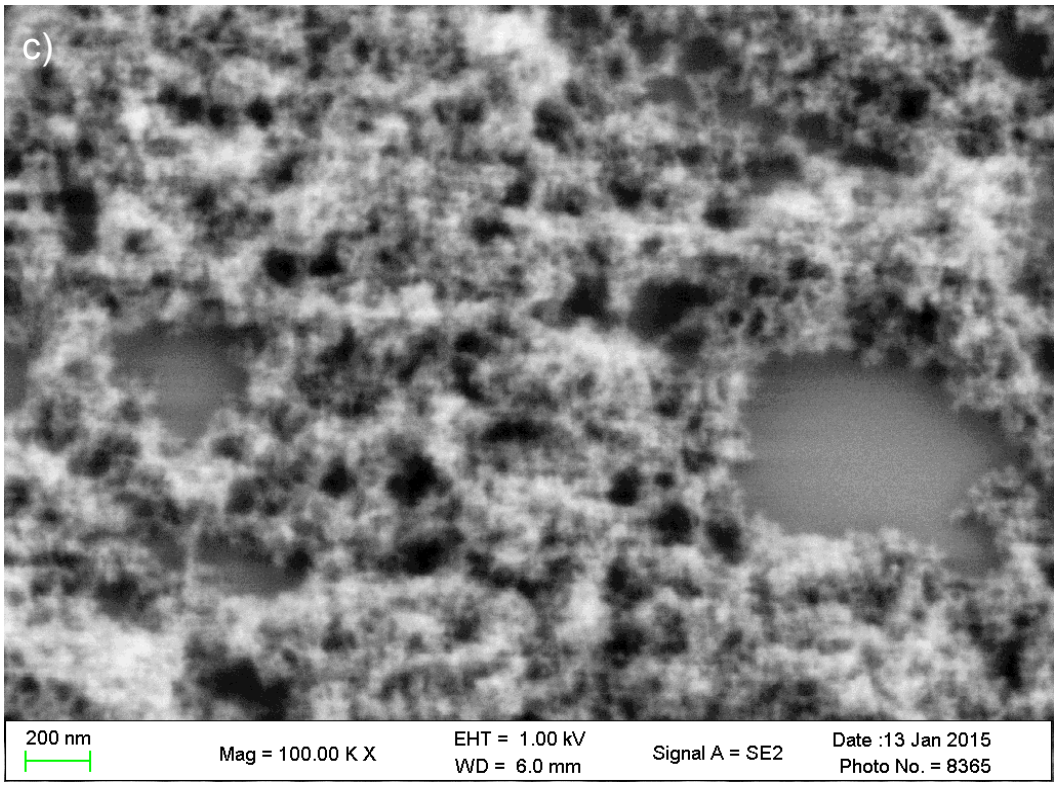
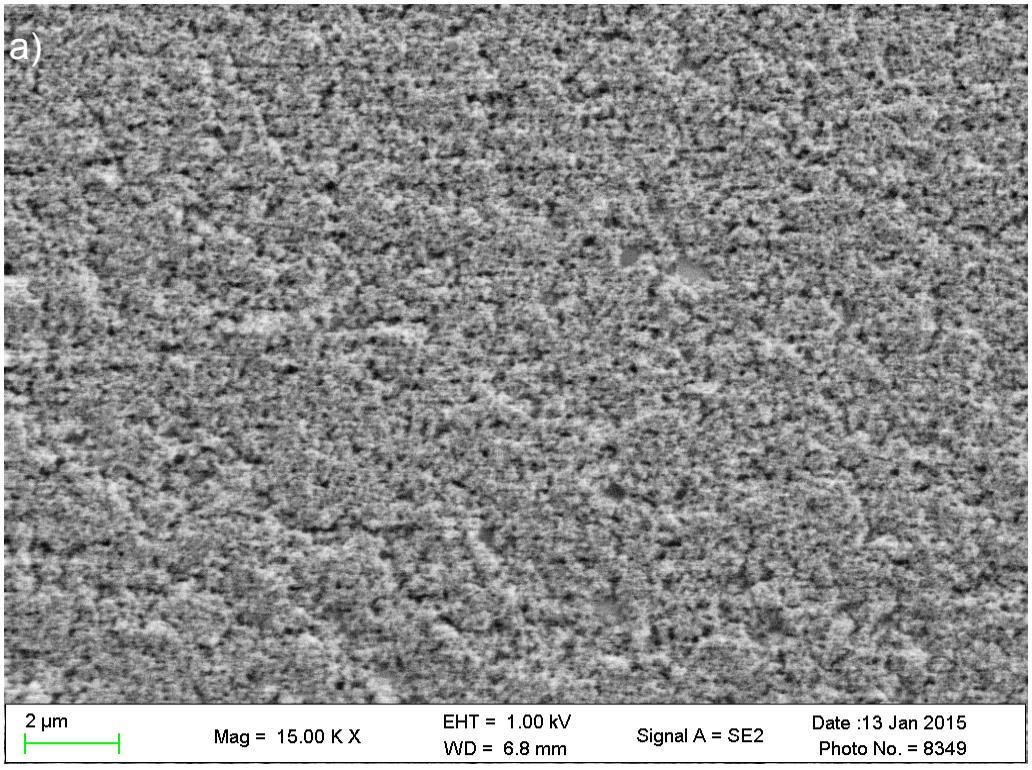


Figure 22 Continued

Figure 23: The SEM micrographs of SHPC 5X coating on a silicon wafer at a) 10KX, b) 25KX, and c) 100KX with indication of coating distribution.



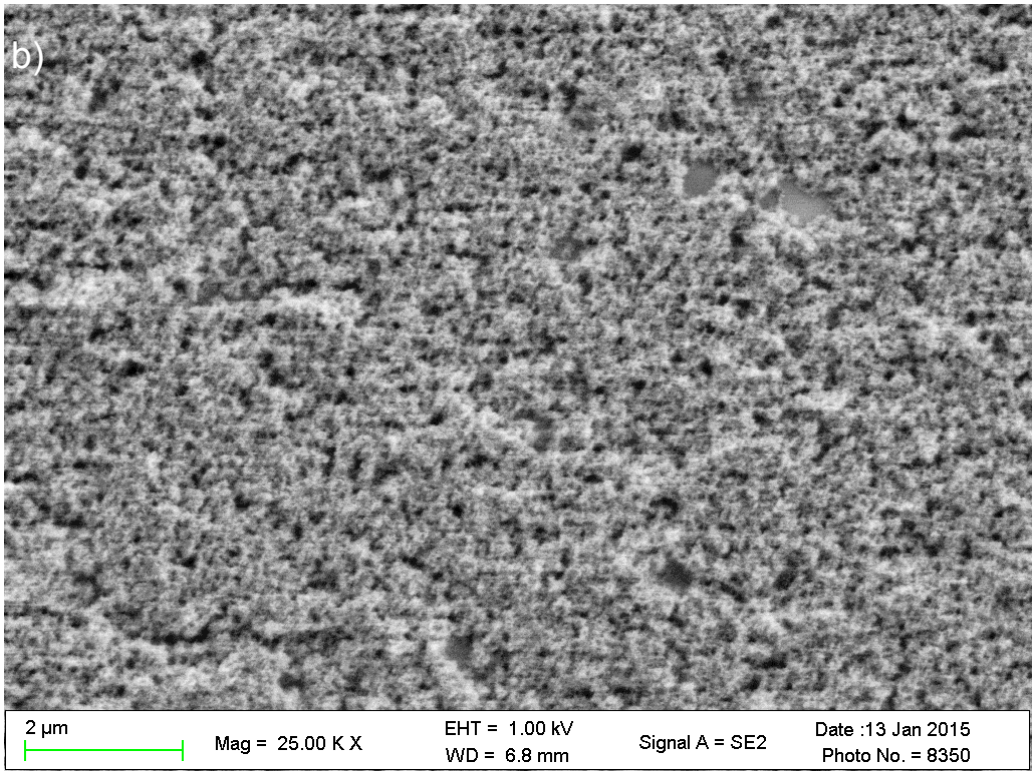


Figure 23 Continued

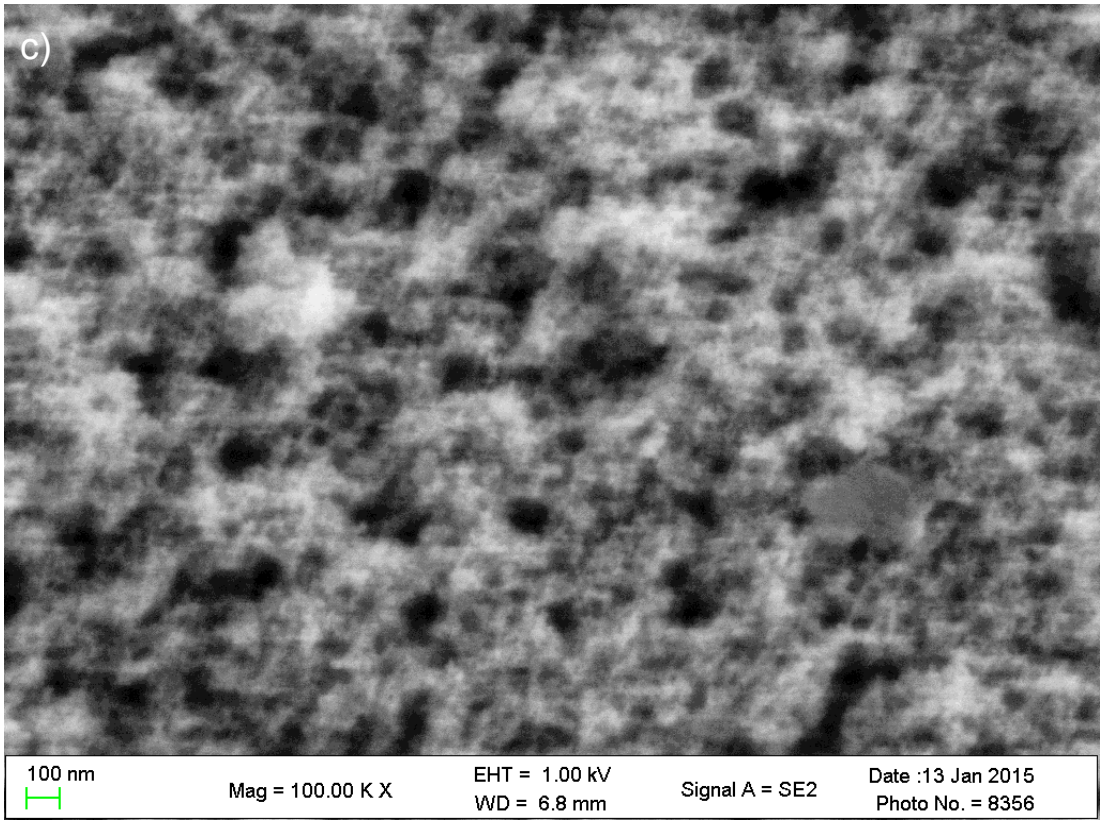
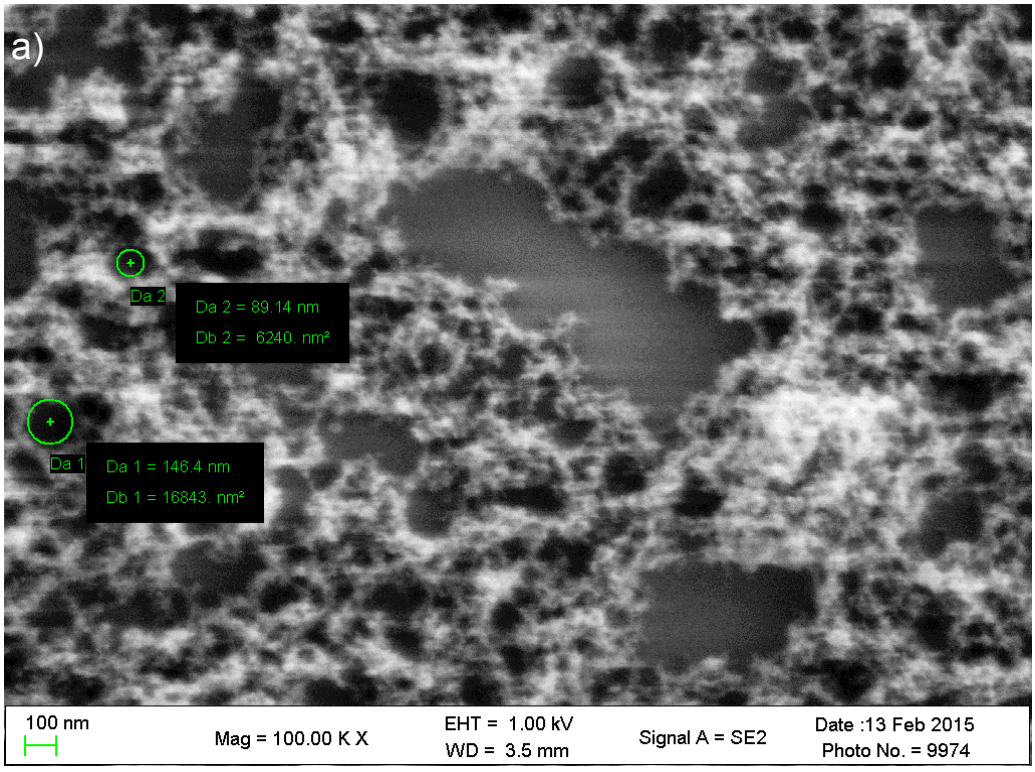


Figure 23 Continued

The SEM images of the different SHPC coatings were also used to determine the pore sizes present on the rough surface of the coating. In Figure 24, the pores were measured using the relative tools found in the SEM software, which resulted in an average pore size of 150nm with rough surface texture surrounding the measured pores size to create a hierarchical structure in the nano-range.

Figure 24: SEM images of (a) SHPC 1X (b) SHPC 3X (c) SHPC 5x coating on a silicon wafer at a 100KX magnification for relative pore size distribution.



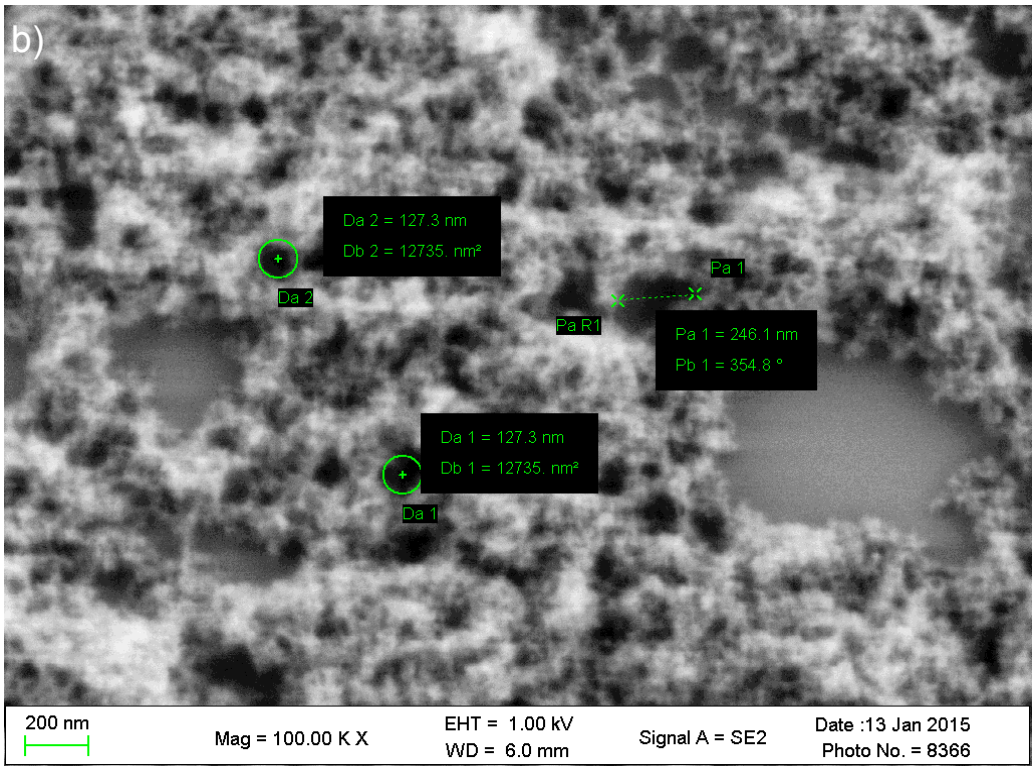


Figure 24 Continued

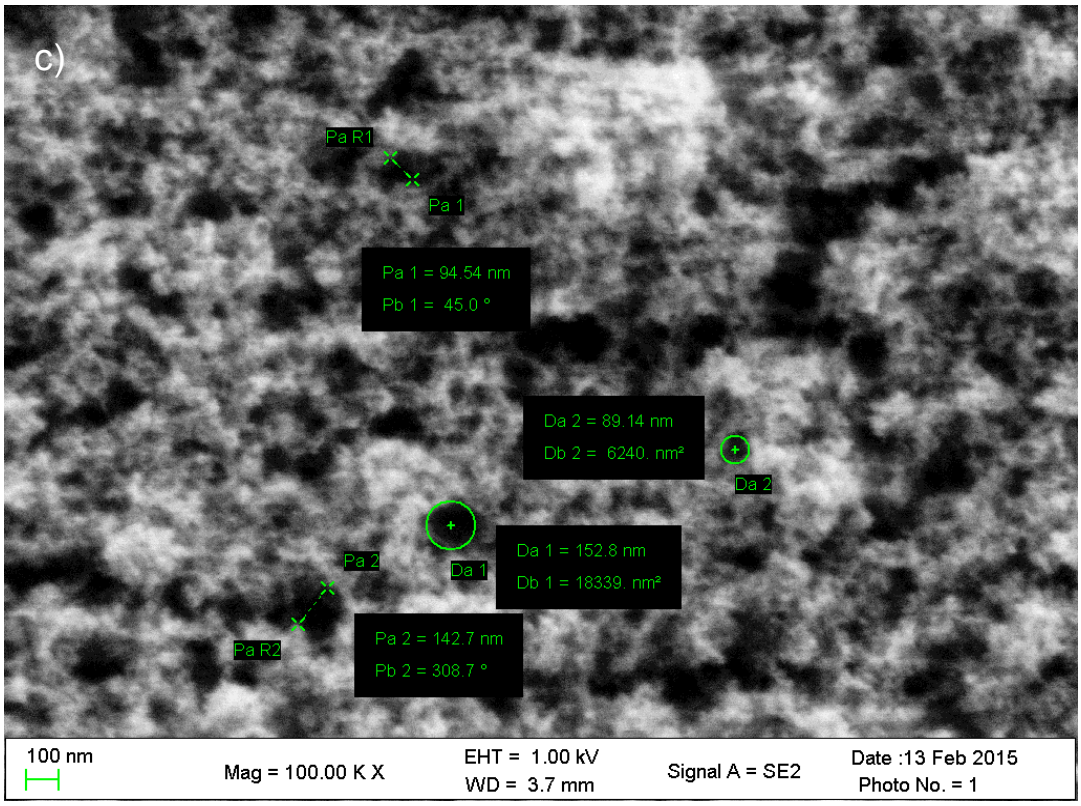


Figure 24 Continued

5.1.3 Surface topography (AFM)

Another technique to further characterize the surface topography of the SHPC coating is atomic force microscopy (AFM). Using a nano-tip in non-contact mode allowed for a scan of the surface topography of the coating in 10µm by 10µm area. The surface topography is presented in a 3-D image that gives a range of the peak height and roughness on the surface. The AFM images (figures 25-27) were obtained for the SHPC 1X, 3X, and 5X coatings. A histogram of the peak heights were also obtained and shown in figure 28. The roughness of the coating had the peaks ranging up to 250nm for SHPC 1X, 500nm for SHPC 3X, and 600nm for SHPC 5X. The peak maximum and minimum for each coating is shown in table 2 along with the average surface roughness of each coating. The average roughness increased with the increase in the coating, which also correlates with the increase in the peak heights.

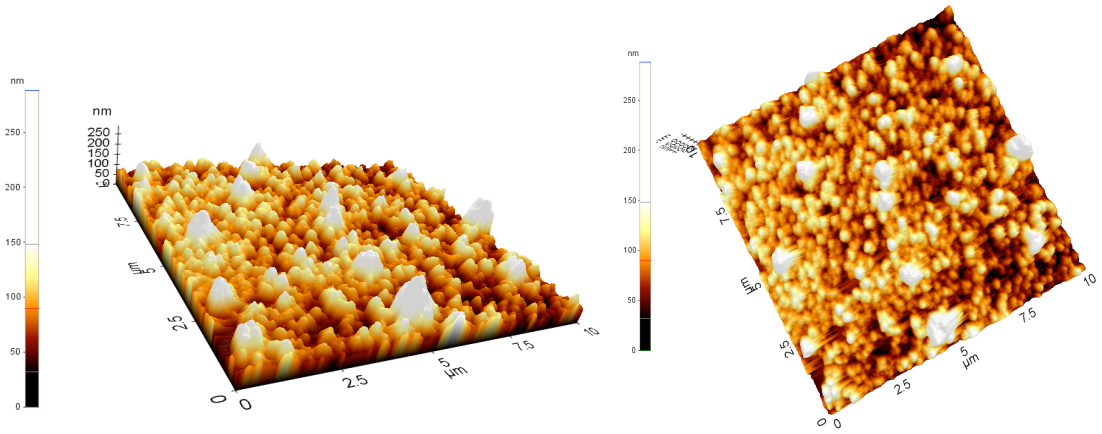


Figure 25: AFM images of SHPC 1X coating on a silicon wafer in a 10µm by 10µm area.

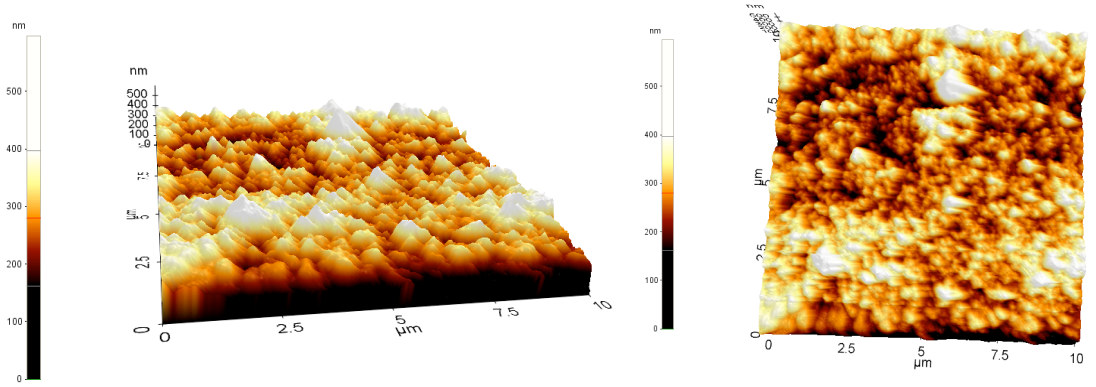


Figure 26: AFM images of SHPC 3X coating on a silicon wafer in a 10µm by 10µm area.

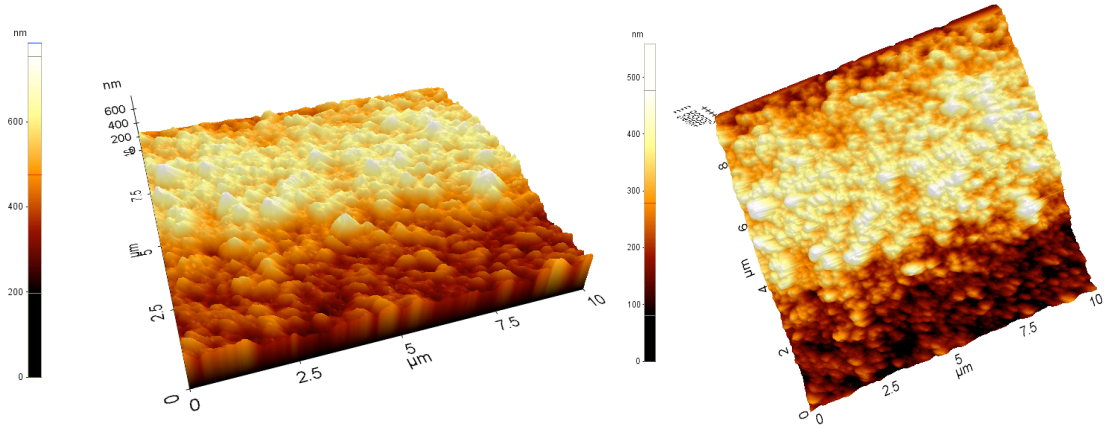


Figure 27: AFM images of SHPC 5X coating on a silicon wafer in a 10µm by 10µm area.

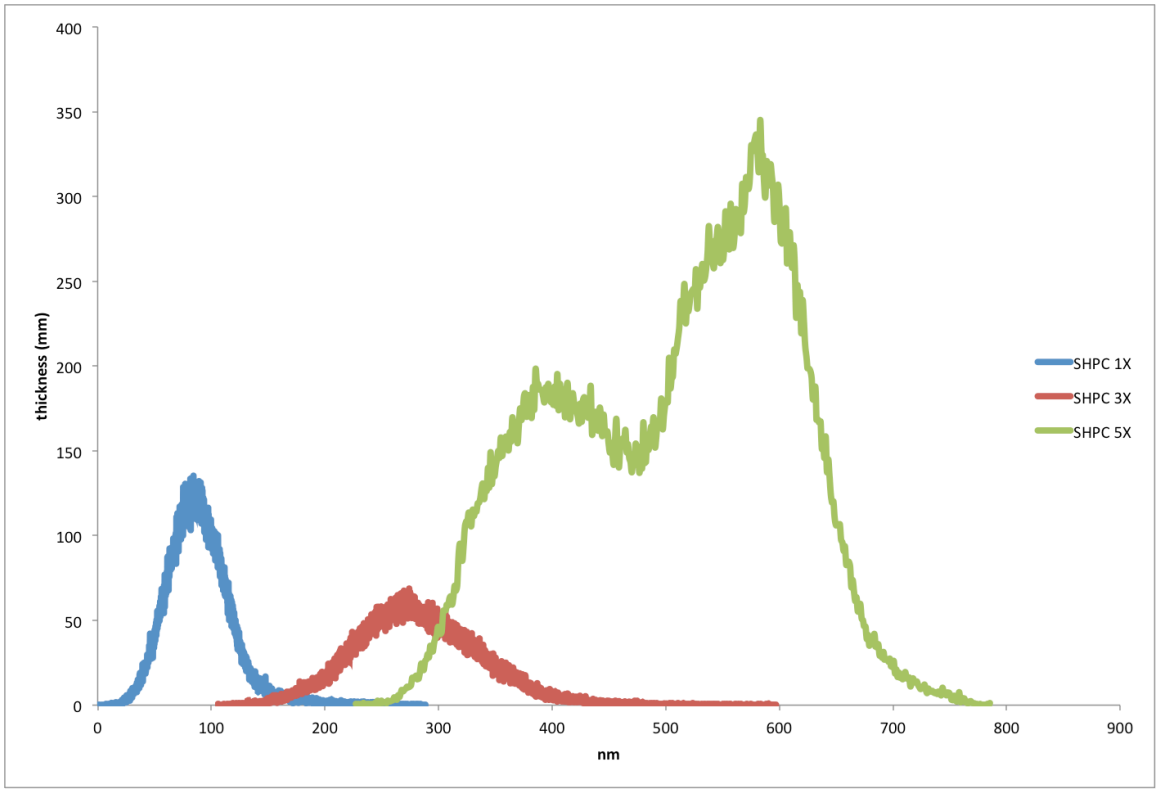


Figure 28: Histogram of the roughness of the SHPC coatings.

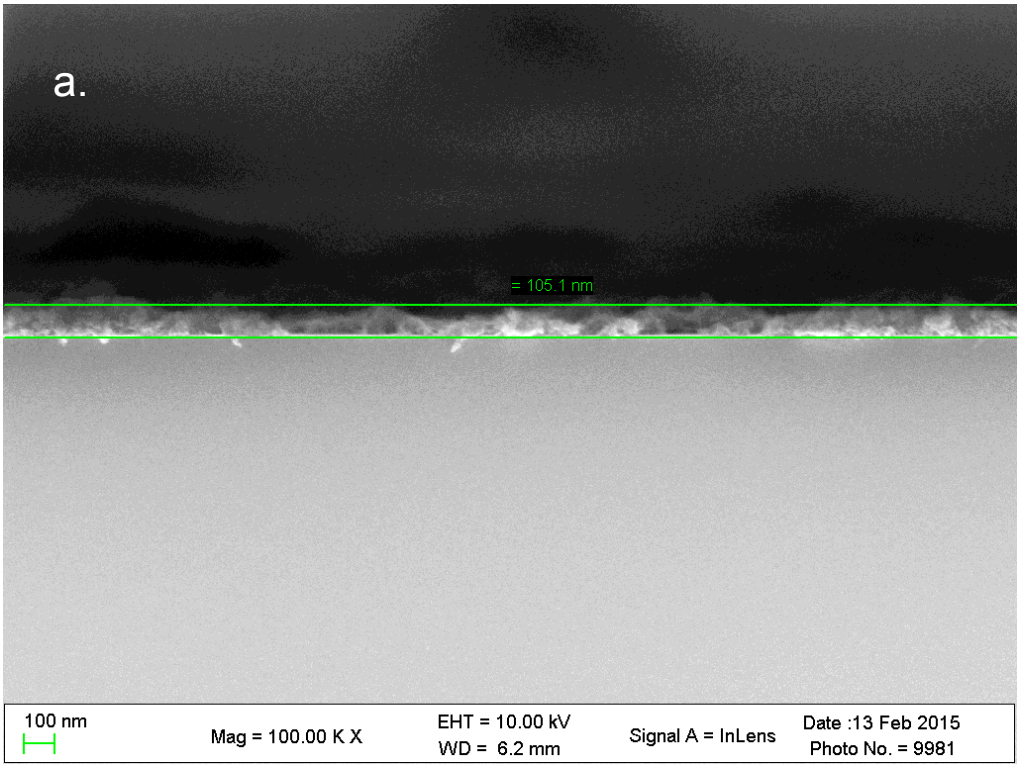
Table 2: The minimum and maximum peak heights in the coating and the average roughness of the SHPC coatings.

	Min(nm)	Max(nm)	Mean(nm)	Ra(nm)
SHPC 1X	0.00	288.63	89.98	22.06
SHPC 3X	105.89	597.04	282.64	44.14
SHPC 5X	226.14	785.43	505.34	86.34

5.1.4 Thickness of the Coating

The AFM images gives an idea of the thickness of each coating through the peak heights, but to confirm the thickness of the coating additional SEM images were taken of fracture surfaces looking at a cross-section of the coating. Silicon wafers were fractured immediately prior to imaging to assure that the fracture surface was not contaminated. The SEM was tilted at 90° and position at the area of the fracture surface. The images are taken with an InLens detector at 10KV at a magnification of 100KX for SHPC 1X, 3X, and 5X coating shown in figure 29. Using the available software tools, thickness of each coating was measured with the SHPC 1X coating having the lowest thickness of 105.1nm and the 5X coating have the highest thickness of 327nm. The thickness of the coating appears to be increasing with the increase in coating layers.

Figure 29: SEM images of (a) SHPC 1X (b) SHPC 3X and (c) SHPC 5X coating on a silicon wafer observed at 100KX.



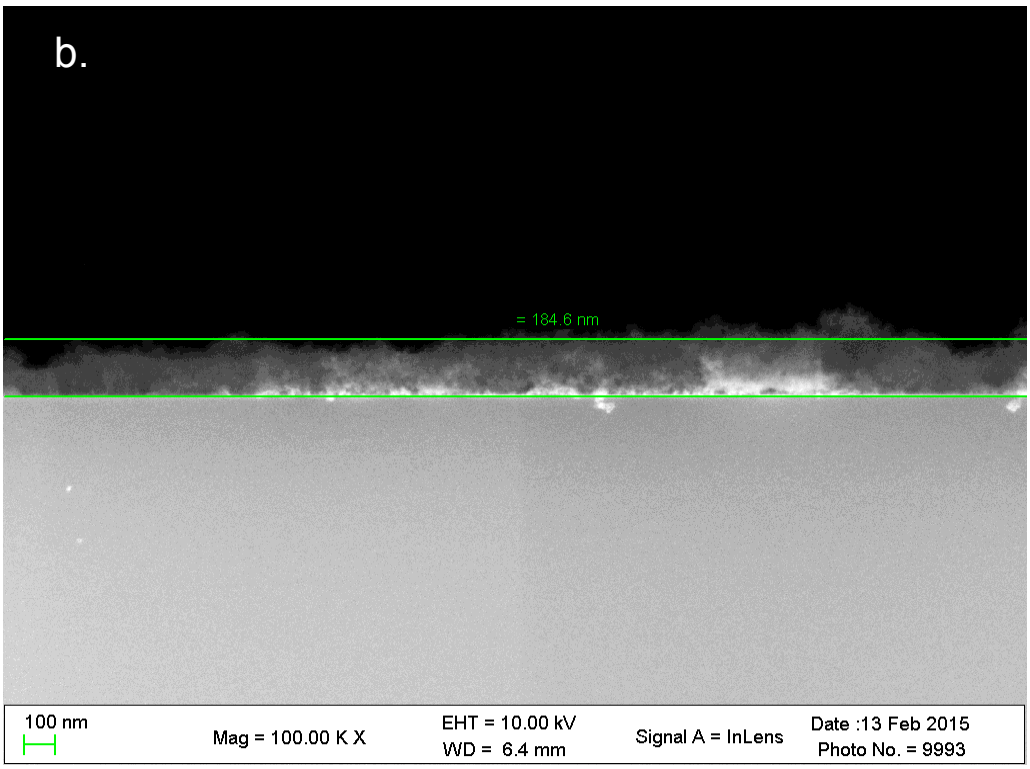


Figure 29 Continued

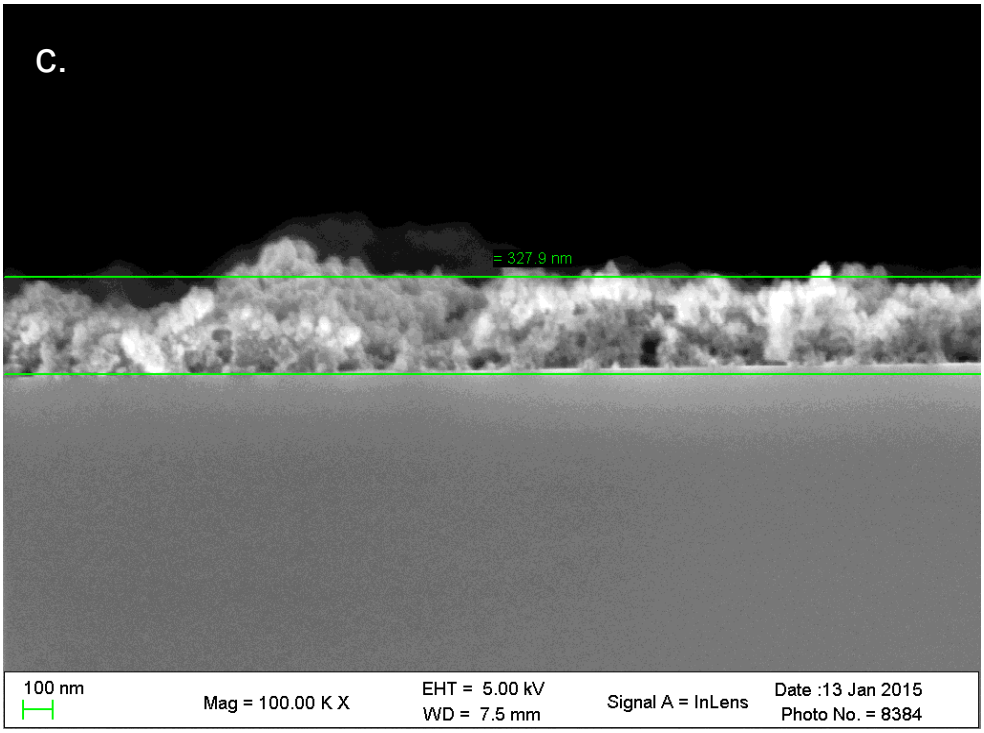


Figure 29 Continued

5.2 Superhydrophobicity

5.2.1 Contact Angle Measurement

The superhydrophobic properties of the coating were measured through contact angles (CA) with two probe liquids: DI water and diiodomethane to calculate the surface free energy of the coating. Five points are measured and the results are shown in table 3. The CA was measured on a quartz glass substrate with no coating as a reference. In figure 30, the CA produced by the polar liquid (DI water) is plotted against the nonpolar liquid (diiodomethane) with the highest contact angle reaching 151° The standard error of the CA measurement for the different coatings were quite small indicating that that the mean value for the CA is an accurate depiction of the CA of the coating. Measurement of the SHPC 10X coating was unattained due to the low adhesion of the water droplets to the surface causing the droplets to roll off the surface. This indicated the possibility of achieving high CA's close to 180° (figure 31). The contact angles were then used in Wu's method to calculate the surface free energy of the coating as well as the work of adhesion of the liquid to surface (table 4).

Table 3. Contact Angle measurement of the SHPC coatings at five different points.

DI water				
	Quartz	SHPC 1X	SHPC 3X	SHPC 5X
1	20	130	150	151
2	21	139	150	150
3	20	136	151	151
4	20	140	150	150
5	20	143	155	150
Diiodomethane				
	Quartz	SHPC 1X	SHPC 3X	SHPC 5X
1	55	42	30	23
2	40	42	20	20
3	50	50	30	21
4	40	50	33	22
5	50	50	33	23

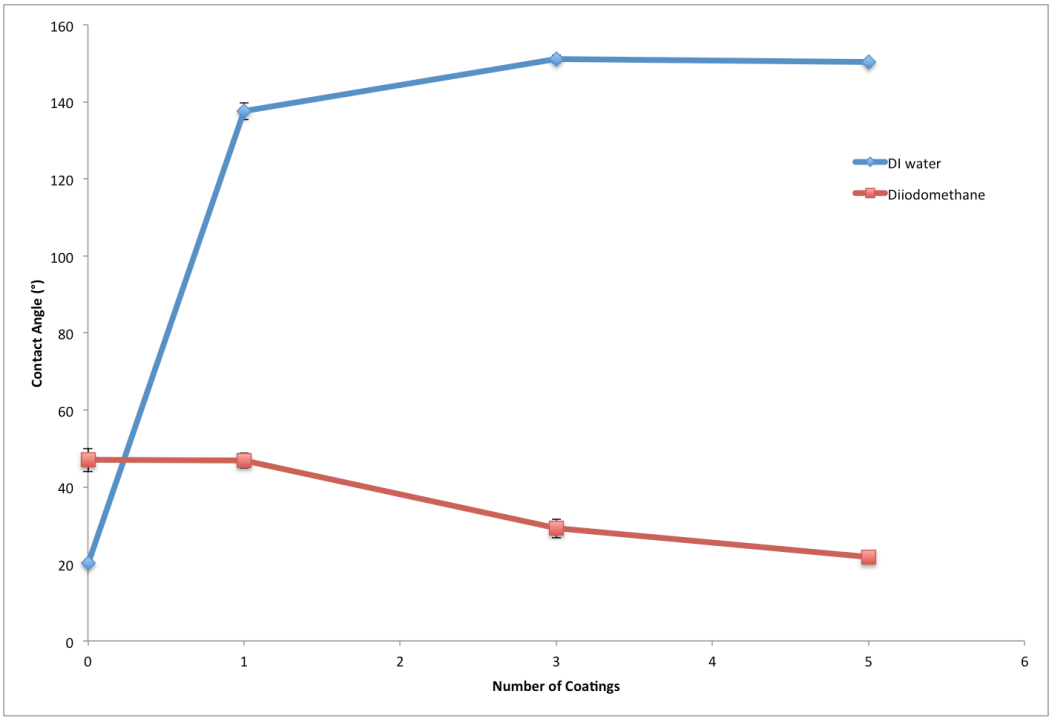


Figure 30: Contact Angle Measurement of different number of coatings with DI water and Diiodomethane probe liquids.

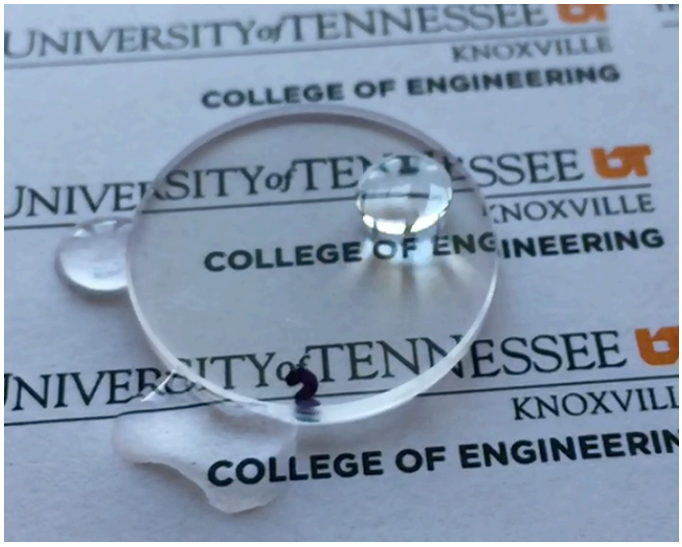


Figure 31: Superhydrophobic polycarbonate coating (SHPC) coated 10 times on a quartz substrate with water rolling off the surface.

Table 4: The Surface free energy obtained through contact angle measurements and the work of adhesion between the liquid and the solid.

	γ_s	γ_d	γ_p	W_a
Quartz	72.20	30.55	41.65	140.15
SHPC 1X	12.41	16.06	-3.65	18.91
SHPC 3X	5.05	8.13	-3.08	9.56
SHPC 5X	4.94	8.01	-3.06	9.44

5.3 Optical Properties

5.3.1 Transmission

The UV-Vis is used to measure the transmission of visible light through the SHPC coating to observe the optical properties in figure 32. Quartz glass is the substrate used for the coating and thus is used as the reference. The transmission was measured in the visible light wavelength range from 800nm to 200nm using a sample holder with an area of 0.5 in^2. The transmission of the quartz reference was approximately 91% and the transmission of the SHPC coatings ranged from 92-93% with only a slight decrease in the transmission between SHPC 1X and SHPC 10X. This decrease is quite small, which results to an insignificant change to the transmission with the increase in the thickness of the coating.

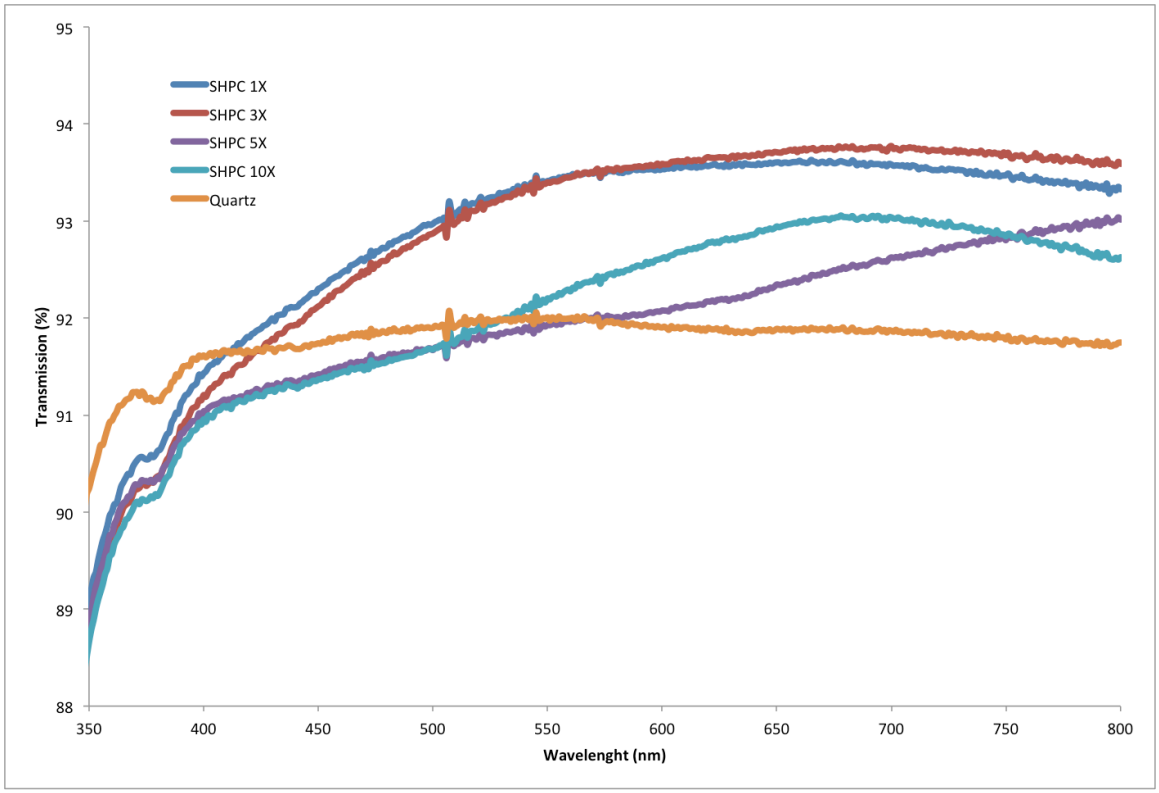


Figure 32: Transmission of SHPC coatings on quartz glass through the visible light range.

5.4 Mechanical Properties

5.4.1 Nanoindentation

The young's modulus of the coating at the twenty points and was averaged out. This figure indicates that the modulus is proportional to the hardness. An upper limit was set at 130 GPa for the substrate (silicon wafer) and a lower limit of 1.9 GPa for matrix of the coating (PC) as shown in figure 33. The modulus of the different SHPC coating appears to fall between the limits.

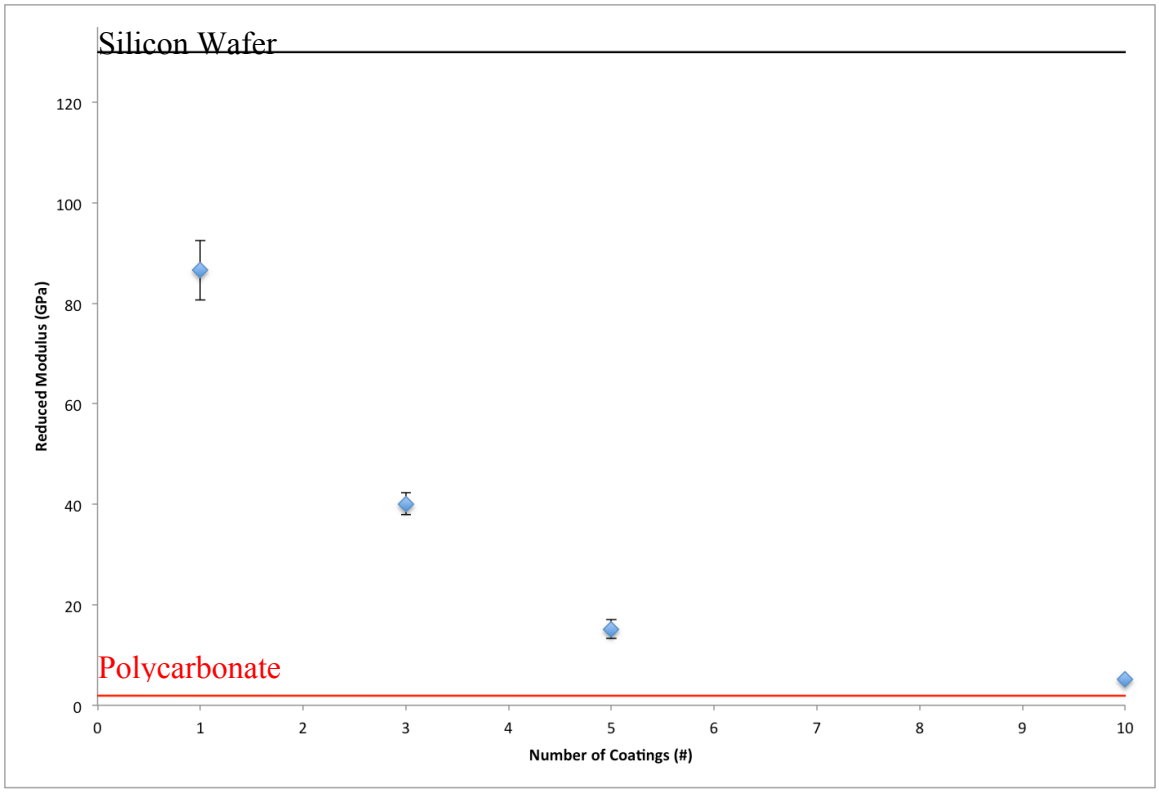


Figure 33: Young's modulus obtained for SHPC 3X, SHPC 5X, and SHPC 10X coating on silicon wafer.

The nanoindentation also measured he hardness of the different coatings at the twenty points were averaged and is shown in figure 34 with the upper limit being that of the substrate (silicon wafer) at 13GPa and the lower limit being the matrix of the coating (PC) at 0.28 GPa. It can be seen that hardness decreased with the increase of the coating. At SHPC 1X and 3X falls between the limits and the SHPC 5X and SHPC 10X appears to have a lower hardness than that of PC.

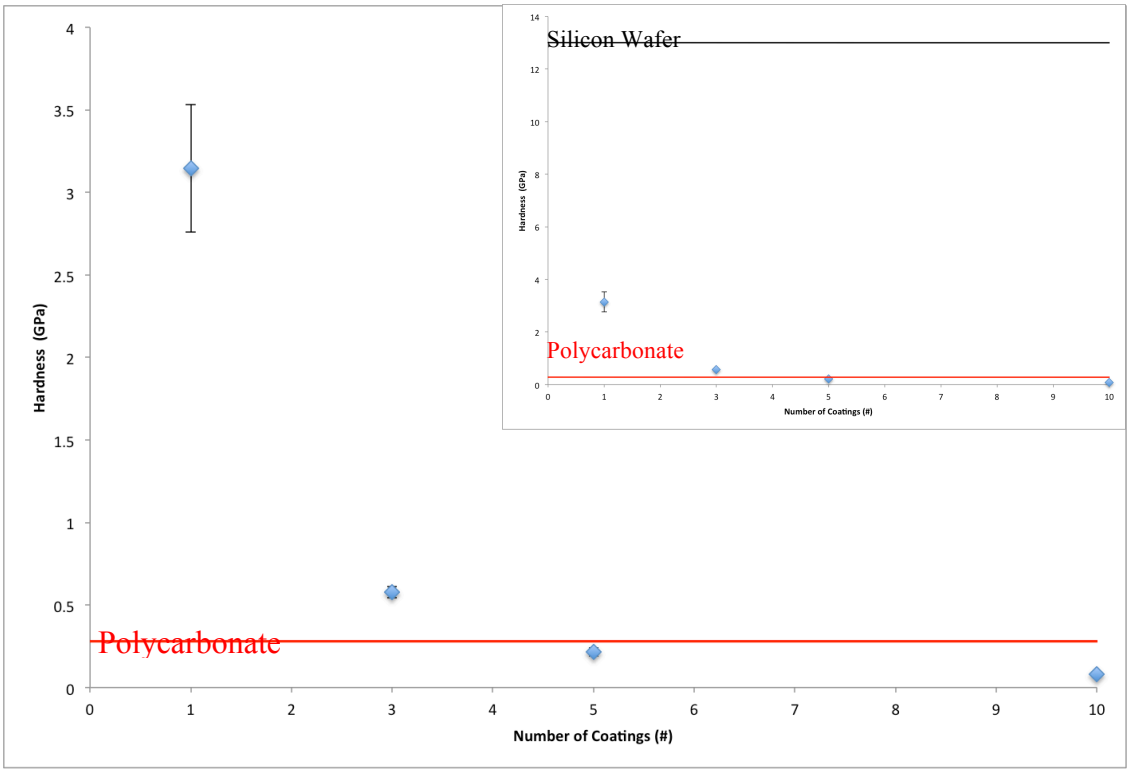


Figure 34: Hardness obtained for SHPC 3X, SHPC 5X, and SHPC 10X coating on silicon wafer.

CHAPTER V
DISCUSSION

The superhydrophobic property of this coating is analyzed for elemental analysis and functional group composition using EDS and FTIR-ATR, respectively. The EDS data in figures 18 and 19 is providing information on elements present in the superhydrophobic polycarbonate coating (SHPC) indicating traces of O, C, and Si. The matrix of the coating is polycarbonate (PC) and thus the presences of C and O are the expected elements for this polymer film. The detection of PC also indicates that during the spin-coating process, the speed of 2500rpms was sufficient enough to evaporate the tetrahydrofuran (THF) solvent and still retain the PC to act as a matrix for the aerogel particles. The amount of oxygen is significantly greater than carbon due to the presences of O in PC as well as in in aerogel, which is composed of silicon dioxide (SiO_2). The largest element concentration found from the EDS measurement was silica and this can be contributed by the aerogel, the silicon substrate, and the silicon x-ray detector. When comparing the superhydrophobic polycarbonate coating with one layer (SHPC 1X) coating (figure 18) and the superhydrophobic polycarbonate coating with ten layers (SHPC 10X) coating (figure 19), it is observed that as the coating increased, the amount oxygen increased and silica decreased by 12% (appendix table 8). This observed effect is due to the change in thickness of the coating. The thickness is dependent on the number of coatings placed on the substrate, thus as the number of coating increase the thickness increase (figure 29). A thicker coating will prevent the beam from penetrating through the coating and on to the substrate giving inaccurate measurements for the concentration of silica. The depth of penetration from the beam is dependent on the accelerating voltage and the density of the material (Equation 16)

$$x(\mu m) = \frac{0.1E_0^{1.5}}{\rho} \qquad (16)$$

where x is the depth of penetration in μm, E_o is the accelerating voltage in keV, and ρ is the density of the material in g/cm^3. Since the film is composed of PC and aerogel nanoparticles both materials contribute to the density. When using Eq. 11 with an acceleration voltage of 5keV, the maximum depth of penetration would 928 nm with a density of 1.21 g/cm^3. Since the SHPC 1X coating is the thinnest coating, with an approximate thickness of 100nm that has a higher silica concentration than the SHPC 10X coating and could be largely from the silicon

wafer substrate. At the SHPC 10X coating, the estimate thickness is 1000nm, which is greater than the beam of penetration resulting in more accurate measurement of the silica concentration in the coating (table 5). This EDS data indicated that the amount of silica was still higher than that of the two other elements present confirming that there is a larger concentration of aerogel compared to PC. This is to be expected due to the 3:1 ratio of aerogel to PC. This also assures that the surface is guaranteed to have aerogel particles present, which is responsible for the superhydrophobic component of the coating.

Table 5: The depth of penetration for EDS compared to the Thickness of the SHPC 1X and SHPC 10X coatings.

	SHPC 1X	SHPC 10X
Depth of Penetration (nm)	928	928
Thickness (nm)	100	1000

Aerogel exhibits the rough nano-structure needed to achieve a superhydrophobic coating; however, it is initially hydrophilic and thus verifying that the surface has been modified to be hydrophobic is crucial. Although the EDS measurement show significant amounts of Si, it did not indicate any functional groups that could lower surface free energy of aerogel such as fluorine groups. Fluorine is an element that has a relatively low x-ray energy, which could cause it to be undetectable by the x-ray beam that has a much larger energy. To confirm the presence of the functionalized aerogel, an FTIR spectrum was obtained for the SHPC coating to obtain a more accurate indication of the functional groups present on the surface of the coating. The spectrum was obtained using ATR, which scans more of the surface to avoid penetration to the substrate. The FTIR spectrum of a SHPC 10X coating in figure 20, supports the EDS analysis of the presences of functional groups containing C, O, and Si. The spectrum also confirms the presences of PC in the coating with the presences of a carbonyl group at 1750 cm^{-1} and a benzene ring stretch at 1510 cm^{-1} [49]. The presences of functionalized aerogel particles were also confirmed with peaks of fluorine at 1299 – 1188 cm^{-1}. The surface composition has been verified contain functional groups that can impact hydrophobic character, but the surface topography must be verified to exhibit the rough hierarchical structure to obtain superhydrophobicity. Similar to the EDS data, the substrate could be measured which could effect the analysis of the functional groups of the SHPC coating. The depth of penetration can be calculated using equation 17

$$dp = \frac{\lambda}{2\pi n_1 \left[\sin^2 \theta - \left(\frac{n_2}{n_1} \right)^2 \right]^{1/2}} \qquad (17)$$

where *dp* is the depth of penetration in nm, λ is the wavelength of IR radiation, n_1 is the refractive index of the ATR crystal which for this work is diamond (2.41), and n_2 is the refractive index of the sample which is the SHPC coating. Since the coating is composed of a PC matrix, the refractive index of PC was used (1.51). The calculated depth of penetration in Table 6 indicates that it is dependent on the wavelength of the IR radiation. It is seen that the longer the wavelength, the deeper the penetration. The depth of penetration for the IR is also dependent on the index of refraction of the ATR crystal. It can be observed that lower refractive index will result in deeper penetration. Since the SHPC 10X sample is estimated to have a thickness of 1000nm, the diamond crystal is ideal for obtaining an FTIR spectrum of the coating.

Table 6: The calculated depth of penetration for ATR

SHPC 10X		
cm^{-1}	λ (nm)	dp (nm)
4000	2500.00	624.80
3500	2857.14	714.05
3000	3333.33	833.06
2500	4000.00	999.67
2000	5000.00	1249.59
1500	6666.67	1666.12
1000	10000.00	2499.19
500	20000.00	4998.37

There were significant changes in the surface roughness between the different coatings of SHPC 1X, 3X, and 5X coating. When comparing the SEM images of these coating it can be seen that the coverage of the substrate increased with the increase in the number of coatings. This is to be expected, as additional layers

will cover the surface that was not covered from the previous layer; however, the addition of these layers on top of one another interfuse with each other rather than sitting on surface of each other as seen in figure 29. The SEM images of the surface of the SHPC 1X, 3X, and 5X coating in figures (21-23) indicate that the average gap distance of each coating correlated with the superhydrophobicity of the coating based of the contact angle (CA) measurements (table 3). As mentioned, most superhydrophobic surfaces exhibit higher CA with a hierarchical structure roughness. Although, there is no report maximum value specified between each gap distance, it could be averaged specifically for this particular coating. In the SHPC 1X coating (figure 21) the gap distance or missing area of coverage, ranges from 1.5 μm to 400nm. The range of separation has proven to be too far apart to obtain a superhydrophobic surface, even with pore sizes ranging between 90nm to 114.6nm. The SHPC 3X coating (figure 22), the gap distance have significantly reduced ranging from 800nm to 500nm and the 5X coating (figure 23) having almost no gap length representing a uniform coating on the surface with complete coverage. The CA measurement obtained for the SHPC 1X coating did not exhibit any superhydrophobicity; however, the SHPC 3X and SHPC 5X coating did exhibit superhydrophobicity with the result of high contact angle of 150°. This indicates that the maximum gap distance to obtain a superhydrophobic coating is 800nm, which is resulted from coating the substrate three times. Further increasing the number of coatings would only assure that the substrate is completely covered and superhydrophobic.

The hierarchical micro-nano structure has been proven to be more effective at achieve a superhydrophobic coating compared to just having a nano-structured or microstructured surface [14]. This is achieved with a gap length produced from different layers of coating. Through the study from the SEM micrographs, it is observed that the superhydrophobicity of the coating is also affected by the porousity of the coating and thus further evaluation of the surface topography is obtained by evaluation of the nano-pore of the coating. Evaluating the pore sizes of the coating indicates additional roughness to the surface with the pore sizes of the SHPC coating ranging from 90nm to 114.6nm (figure 24). It is observed that the porosity of the coating is not affected by the change in the number of coatings or thickness. This is due to the porous structure of the aerogel, which exhibits the nano-structure to obtain superhydrophobicity. This proves that the SHPC 1X coating still exhibit higher contact angles than the quartz glass (table 3) due to the initial layer of nano-structured roughness on the surface. By increasing the thickness of the coating, the micro-component of the hierarchical structure is also obtained while still having the nano-structured component. Surrounding the

pores is a cloud like texture that represents even smaller nano-features that again creates another hierarchical structure, but in the nano-range for a superhydrophobic surface. In figure 35, the result of water interacting with a SHPC surface would present similar behavior shown in the Cassie-Baxter model, where a rough surface with low surface free energy will raise the liquid to reduce contact with the surface creating two interfaces (liquid-air and solid-air).

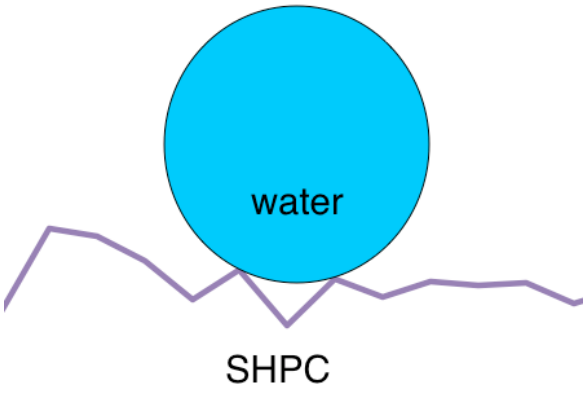


Figure 35: An illustration of the SHPC coating when water is on the surface

The SEM images indicated the presences of hierarchical structures on the surface, but to assure that the surface is roughen AFM is obtained for SHPC 1X, 3X, and 5X coatings (Figure 25-27). The AFM images of a 10μm by 10μm area displays that the surface the coating was roughen in all the coatings. Table 2 indicates the maximum and minimum peak of the coatings with SHPC 1X having the lowest at 0nm and SHPC 5X having the highest peak at 785nm. The AFM images supports the SEM micrographs of the coatings (figure 21-23). The presence of a 0nm peak indicates there was no coverage in the area that was observed in the SEM micrograph for SHPC 1X in figure 21a. It can be seen that increasing the number of coatings leads to an increased peak heights. The average value of the peaks as well as the average roughness of the coatings is also shown in table 2. Averaging the peak heights will present an idea of the general thickness of the coating, which is similar to the thickness values obtained for the different coatings in figure 29. The roughness average (Ra) is an arithmetic average of the surface peaks and valleys shown in equation 18:

$$R_a = \frac{1}{n}\sum_{i=1}^{n}|y_i| \qquad (18)$$

where n is the number of peaks and y_i is the absolute value of the peak heights deviation from the mean [ASTM B46.1]. The average roughness of the surface and is shown to have increase with the increase in the coating with the largest roughness having a value of 86.34nm. This is to be expected for the addition of coatings creates an infused thick layer resulting in more coverage of the surface and thus more roughness to the surface.

The size of the aerogel particles is a significant aspect to creating a transparent superhydrophobic coating. The size of the particles must be lower than that of the visible light range (700nm to 200nm) to exhibit transparency. The SEM images of the aerogel can be described, as a porous mesh that appears to have pores no larger than 250nm. This indicates that the transparent aspect of the coating is possible, especially in the higher wavelengths, and should correlates with the transmission of the coatings. The addition of coatings creates a thicker coating on the surface that could diminish the transparent component of the coating. The transmission of the SHPC 1X coating in figure 32 is approximately 93% ±0.3% and appears to decrease slightly with the increase in coatings, which is proportional to the thickness of the coating. The result of the high transmission could also indicate anti-reflective properties the coating. Since the addition of coating produces an infused thicker layer, the nano-aerogel particles can have the possibility to conglomerate forming larger particles that can scatter light. At SHPC 10X coating, the transmission appears to lower slightly to 92 ±0.4%, but is still higher than the transmission of the quartz glass (91% ±0.4%). This indicates there would need to a significant amount of coatings on the substrates to even obtain the transmission of quartz glass and since the superhydrophobic property of this coating can be achieved with three to five coatings there is presently no need to add additional layers.

Contact angle (CA) measurement is the method known to determine the superhydrophobicity of a coating and to obtain the surface free energy. A surface is determined to be superhydrophobic if the CA is equal to or greater than 150°. The measurements of the SHPC 3X and 5X coatings obtained this value (table 3). The volumes of the droplet of the probe liquid when measuring CA are typically 1µL to 5µL to obtain accurate values; however, for this measurement the volume of the droplet was 25µL to 30µL. When attempting to measure CA with

the smaller volume, the droplet would not adhere to the surface to obtain measurements, thus larger droplets were used. The increase in the volume of the droplet causes inaccurate measurements of the CA due to the effects of gravity acting on the large droplets as compared to small droplets where gravity is less of a factor. Despite having larger volume droplets, the CA obtained were still 150°, which indicates that the CA could possibly be greater when measured with smaller volume liquids.

Using Young's equation and relating that to the work of adhesion and Wu's method for determining surface free energy, the surface free energy is obtained for the coating and the interfacial free energy between the probe liquids and the coating. It appears that the surface free energy of the SHPC 1X coating is 12.41 mN/m and the SHPC 3X and 5X coating has similar surface free energy of 4.72 and 4.94 mN/m. All the surface free energy of the SHPC coatings were significantly lower than that of quartz glass, which had a surface free energy of 72.2 mN/m as shown in table 3. The surface free energy is composed of a dispersive component and a polar component and using the probe liquids (diiodomethane and DI water) these components were measured with negative polar components for the SHPC 3X and 5X. The dispersive component are composed of London-dispersive forces that are depended on the dipole-moment and thus there is no possibility to obtain a negative dispersive force; however, the polar component is composed of acid-base interaction which deals with electron donors and electron acceptors. With this component the possibility of obtaining a negative value is possible due to the possibility of obtain more acids than bases or vise versa. The surface free energy is a reflection of the superhydrophobicity of the coating and as mentioned a SHPC 3X coating is the minimum coating required to obtain this property. The work of adhesion between the liquid and the solid was also obtained and proved to be proportional to the surface free energy with work of adhesion decreasing with the increase in the number of coatings. This decrease is again due to the low surface free energy of the surface. When measuring the CA for the SHPC 10X coating for DI water, the water would roll off the surface (figure 31). This could indicate that the CA is close to 180°. When calculating the work of adhesion of higher CA values (Table 7), the resultant work of adhesion were relatively low and at 180° the value was 0.00mN/m. This indicates that there is no adhesion between the water and the substrate causing the water to roll of the surface. However, there is still a small amount of surface free energy present due to the dispersive forces produced from dipole moments.

Table 7: Estimated surface free energy and work of adhesion for SHPC 10X

SHPC 10X			
CA	170	175	180
γ_s	1.22	0.91	0.80
γ_d	4.20	3.88	3.76
γ_p	-2.98	-2.97	-2.96
W_a	1.10	0.28	0.00

The mechanical properties are measured for the transparent coating using nanoindentation. The technique revealed the hardness and young's modulus of the coating. The twenty points measured reveals that the mechanical properties of the sample are largely impacted by the thickness. As the coating increases along with thickness, the hardness and modulus decreases. This is due to the thickness of the sample and the depth of penetration. It is shown in the SEM images that the thickness of the coating increases with the coating and that the minimum thickness is 100nm (figure 29). Since the coating is placed on a silicon wafer substrate, the hardness and the modulus should not be greater than that of a silicon wafer or less than that of PC, which is the matrix of the coating. The indenter could have penetrated through the coating and onto the surface giving an inaccurate measurement of the hardness and modulus of the coating by accounting for the substrate, but as the coating increases the distances between the coating and the substrate increases creating more accurate measurement of the coating.

The Young's modulus obtained from the measurement shows that the SHPC coatings fell within the limits of the silicon wafer substrate and the PC (figure 33). Young's modulus is indicating the stiffness in the elastic region, which does not experience any yielding to the surface and thus was placed in the designated limit of the silicon wafer and the PC. In figure 34, the hardness for the SHPC 1X and 3X falls between the limits of the silicon wafer (substrate) and the PC (matrix); however, the SHPC 5X and 10X falls below the hardness of PC. The SHPC coatings are shown to have a rough surface topography and with the increase in the coating the average roughness increases (table 2). A rough surface (figure 35) has the possibility of obtaining lower values of hardness compared to a smooth surface due to the air pockets present in the surface. This indicates that part of the measurement during indentation is measuring air resulting in lower hardness values than the matrix material PC.

CHAPTER VI
CONCLUSIONS AND FUTURE WORK

6.1 Conclusions

This work presents a simple and effective method to create these transparent superhydrophobic coatings that has the potential to be applied to a variety of different substrates (glass and polymers). It was also discovered the best overall properties of a transparent superhydrophobic coating can be obtained by applying three to five coats onto the substrate. The EDS measurement indicated the presences of PC and aerogel in the coating and FTIR confirmed that the aerogel was functionalized with fluorine groups. The surface roughness was also confirmed using AFM indicating that the average roughness would increase with the increase in thickness of the coating. These results supported the SEM micrographs, which indicated the increase in the coverage of the coating with the increase in the thickness. The superhydrophobicity of the coating was measure using CA, which obtained values of 150° or higher for the SHPC 3X coating and up. The SHPC coatings exhibit good optical transparency that had higher values close than quartz glass indicating possible anti-reflective properties as well. The hardness and modulus of the coating proved to correlate with the increase in the coating. The hardness was significantly lower than PC, which could be due to the roughness of the coating. A transparent superhydrophobic polycarbonate coating has the potential to be one of the first transparent superhydrophobic coatings that can be applied to wide range of applications. Although the combination of a rough surface topography with the right chemistry has shown to be the important components to achieving a superhydrophobic surface, it has been shown that introducing a transparent component has not jeopardized the superhydrophobic property.

6.2 Future Work

Although this study has shown some advancement in the field of transparent superhydrophobic coatings, there are still several other experiments required before commercialization of this technology. The expansion of this material to larger surfaces is one of the important tasks to optimizing this coating. So far, the method used to apply this coating on substrates is spin coating and has been shown to be an efficient method for small substrates; however, to utilize this technology on larger surfaces perhaps a spray coating method could be explored. Another component for optimization is the fabrication time of the

coating. Currently it has been explored that it takes 24 hours to initially mill the aerogel into nano-sized particles, lowering the milling time could be a huge contribution in creating more coatings in less time. Mechanical properties of hardness and modulus were obtained for the coating, but an important aspect to all coating is the adhesion strength and durability of the coating. The adhesion strength between the surface and coating can be measured and then compared to calculated values using similar equations mentioned in this work. The durability can be a difficult property to obtain due to the transparent property of the coating, but using standard ASTM methods such as a scratch test could be sufficient enough to get an approximation of the durability of the coating. It was observed that the durability of the coating was quite low and could be removed by simply rubbing the surface and thus to create a more durable coating surface modifications can be applied toward substrates introducing functional groups to the substrate that would can form potential covalent bonds to the coating.

LIST OF REFERENCES

[1] X.J. Feng, L. Jiang, Advanced Materials 18 (2006) 3063-3078.
[2] D.W.V. Krevelen, Properties of Polymers - Their Estimation and Correlation with Chemical Structure, Elsevier Scientific New York, 1976.
[3] Y.L. Yuan, Randall, Contact Angle and Wetting Properties, in: G.H. Bracco, Bodil (Ed.) Surface Science Techniques, Springer Berlin; New York, 2013.
[4] A.B.D. Cassie, S. Baxter, Transactions of the Faraday Society 40 (1944) 546-551.
[5] R.N. Wenzel, Industrial & Engineering Chemistry 28 (1936) 988-994.
[6] S. Wu, Journal of Polymer Science Part C: Polymer Symposia 34 (1971) 19-30.
[7] S. Wu, The Journal of Adhesion 5 (1973) 39-55.
[8] M.E.K. Richard M Pashley, Applied Colloid and Surface Chemistry, John Wiley & Sons, Ltd, 2004.
[9] T. Yasuda, T. Okuno, H. Yasuda, Langmuir 10 (1994) 2435-2439.
[10] L. Feng, S. Li, Y. Li, H. Li, L. Zhang, J. Zhai, Y. Song, B. Liu, L. Jiang, D. Zhu, Advanced Materials 14 (2002) 1857-1860.
[11] M. Nosonovsky, Nature 477 (2011) 412-413.
[12] A.P.G. Arthur W. Adamson, Physical Chemistry of Surfaces, John Wiley & Sons, Ltd, 1997.
[13] A. Lafuma, D. Quere, Nat Mater 2 (2003) 457-460.
[14] C. NEINHUIS, W. BARTHLOTT, Annals of Botany 79 (1997) 667-677.
[15] S. Herminghaus, EPL (Europhysics Letters) 52 (2000) 165.
[16] A.R. Parker, C.R. Lawrence, Nature 414 (2001) 33-34.
[17] X. Gao, L. Jiang, Nature 432 (2004) 36.
[18] W. Lee, M.K. Jin, W.C. Yoo, J.K. Lee, Langmuir 20 (2004) 7665-7669.
[19] T. Wagner, C. Neinhuis, W. Barthlott, Acta Zoologica 77 (1996) 213-225.
[20] M.E. Abdelsalam, P.N. Bartlett, T. Kelf, J. Baumberg, Langmuir 21 (2005) 1753-1757.
[21] G. Zhang, D. Wang, Z.-Z. Gu, H. Möhwald, Langmuir 21 (2005) 9143-9148.
[22] J. Zhang, L. Xue, Y. Han, Langmuir 21 (2005) 5-8.
[23] S. Li, H. Xie, S. Zhang, X. Wang, Chemical Communications (2007) 4857-4859.
[24] J. Zimmermann, F.A. Reifler, G. Fortunato, L.-C. Gerhardt, S. Seeger, Advanced Functional Materials 18 (2008) 3662-3669.
[25] M. Ma, R.M. Hill, Current opinion in colloid & interface science 11 (2006) 193-202.
[26] D.E. Bergbreiter, K.-S. Liao, Soft Matter 5 (2009) 23-28.
[27] F. Shi, Z. Wang, X. Zhang, Advanced Materials 17 (2005) 1005-1009.
[28] W. Ming, D. Wu, R. van Benthem, G. de With, Nano Letters 5 (2005) 2298-2301.
[29] S. Amigoni, E. Taffin de Givenchy, M. Dufay, F. Guittard, Langmuir 25 (2009) 11073-11077.
[30] C.-H. Xue, S.-T. Jia, J. Zhang, J.-Z. Ma, Science and Technology of Advanced Materials (2010).
[31] J.T. Han, Xu, K. Cho, Langmuir 21 (2005) 6662-6665.

[32] N.J. Shirtcliffe, G. McHale, M.I. Newton, C.C. Perry, Langmuir 19 (2003) 5626-5631.
[33] Q. Xie, G. Fan, N. Zhao, X. Guo, J. Xu, J. Dong, L. Zhang, Y. Zhang, Advanced Materials 16 (2004) 1830-1833.
[34] P.A. Levkin, F. Svec, J.M.J. Fréchet, Advanced Functional Materials 19 (2009) 1993-1998.
[35] M.N.a.B. Bhushan, Multiscale Dissipative Mechanisms and Hierarchical Surfaces- Friction, Superhydrophobicity, and Biomimetics, Springer New York, 2008.
[36] R. Blossey, Nat Mater 2 (2003) 301-306.
[37] C.S. Gudipati, J.A. Finlay, J.A. Callow, M.E. Callow, K.L. Wooley, Langmuir 21 (2005) 3044-3053.
[38] R.L. Townsin, Biofouling 19 Suppl (2003) 9-15.
[39] A. Marmur, Biofouling 22 (2006) 107-115.
[40] X. Zhang, F. Shi, J. Niu, Y. Jiang, Z. Wang, Journal of Materials Chemistry 18 (2008) 621-633.
[41] P.M. Barkhudarov, P.B. Shah, E.B. Watkins, D.A. Doshi, C.J. Brinker, J. Majewski, Corrosion Science 50 (2008) 897-902.
[42] L. Cao, A.K. Jones, V.K. Sikka, J. Wu, D. Gao, Langmuir 25 (2009) 12444-12448.
[43] W.D. Callister, Materials Science and Engineering: An introduction, John Wiley & Sons, New York, 2008.
[44] G. Abts, T. Eckel, R. Wehrmann, Polycarbonates, Ullmann's Encyclopedia of Industrial Chemistry, Wiley-VCH Verlag GmbH & Co. KGaA, 2000.
[45] V. Serini, Polycarbonates, Ullmann's Encyclopedia of Industrial Chemistry, Wiley-VCH Verlag GmbH & Co. KGaA, 2000.
[46] A. Ram, O. Zilber, S. Kenig, Polymer Engineering & Science 25 (1985) 535-540.
[47] G. Tjandraatmadja, L. Burn, M. Jollands, Polymer degradation and stability 78 (2002) 435-448.
[48] A. Rivaton, Polymer Degradation and Stability 49 (1995) 163-179.
[49] L.J. Bellamy, The Infrared Spectra of Complex Molecules, Chapman and Hall Ltd, London and USA, 1975.

APPENDIX

Early results (Thermal Stability)

During the development of this superhydrophobic polycarbonate coating (SHPC), there were several indication of the thermal stability of the particles. During the ball-milling and sonication process, it was noticed that the aerogel particles would degraded with the increase in heat to the system causing a color change from clear to grey. This indicated that the heat produced from the ball milling and sonication process resulted in elevated temperatures that degraded the aerogel. Despite the color change in the aerogel, it was spin coated on to quartz substrate for initial indication of loss in transparency. The transparency did not seem to be effected by the grey particles as each layer placed on the substrate were in the range of 100nm. When the superhydrophobicity of the coating was measured by placing water droplets on the surface, the water did not roll of the surface or produce high contact angles. This indicating that the heat that resulted in the color change of the aerogel particles also eliminated the functionalized component of the aerogel. Through these observations, additional precaution to lowering the speed of the ball-milling process and keeping the solution cooled in an ice bath during the sonication process was determined.

Table 8: The EDS chemical composition for SHPC 1X and SHPC 10X

SHPC 1X			
Element	Intensity	Weight (%)	Atomic (%)
C K O K Si K	0.78 2.11 1.21	8.14 4.60 87.26	16.64 7.06 76.30
Total		100.00	
SHPC 10X			
Element	Intensity	Weight (%)	Atomic (%)
C K O K Si K	0.85 2.17 1.19	8.39 16.29 75.32	15.88 23.15 60.97
		100.00	

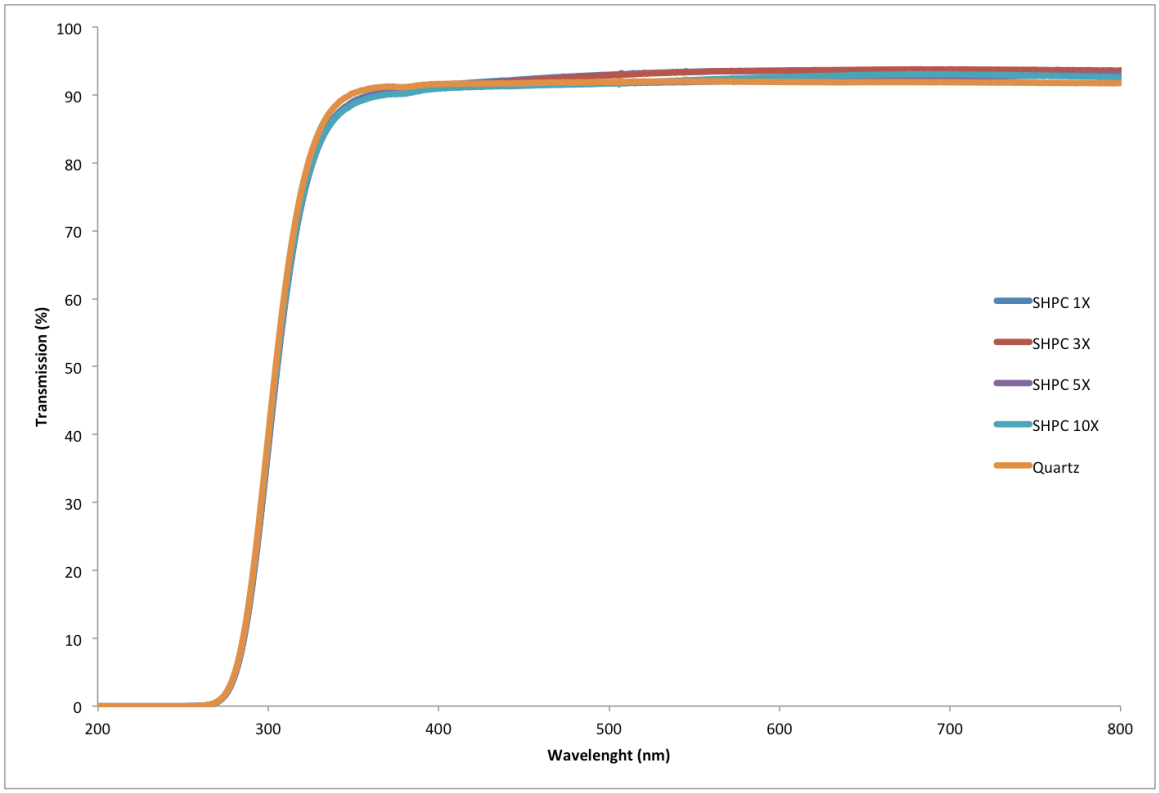


Figure 36: The transmission of the SHPC coatings from 800nm to 200nm.

Table 9:The calculated surface free energy

Surface Free Energy (mN/m)			
Liquid	Surface Free Energy (γ_s)	Dispersive Part (γ_d)	Polar Part (γ_p)
Water	72.3	18.7	53.6
Diiodomethane	50	47.4	2.6
SHPC	γ_s	γ_d	γ_p
Quartz	72.20	30.55	41.65
SHPC 1X	12.41	16.06	-3.65
SHPC 3X	5.04	8.13	-3.09
SHPC 5X	14.94	8.01	-3.06
SHPC 10X (170°)	1.22	4.20	-2.98
SHPC 10X (175°)	0.91	3.88	-2.97
SHPC 10X (180°)	0.80	3.76	-2.96

Table 10: Estimated adhesion strength

Adhesion Strength			
	Contact Angle (°)	γ_s (J/m^2)	W_a (J/m^2)
SHPC 1X	120	12.41	-811.39
SHPC 3X	151	5.05	-287.36
SHPC 5X	151	4.94	-279.53
SHPC 10X	170	1.22	-14.66
	175	0.91	7.41
	180	0.80	15.24

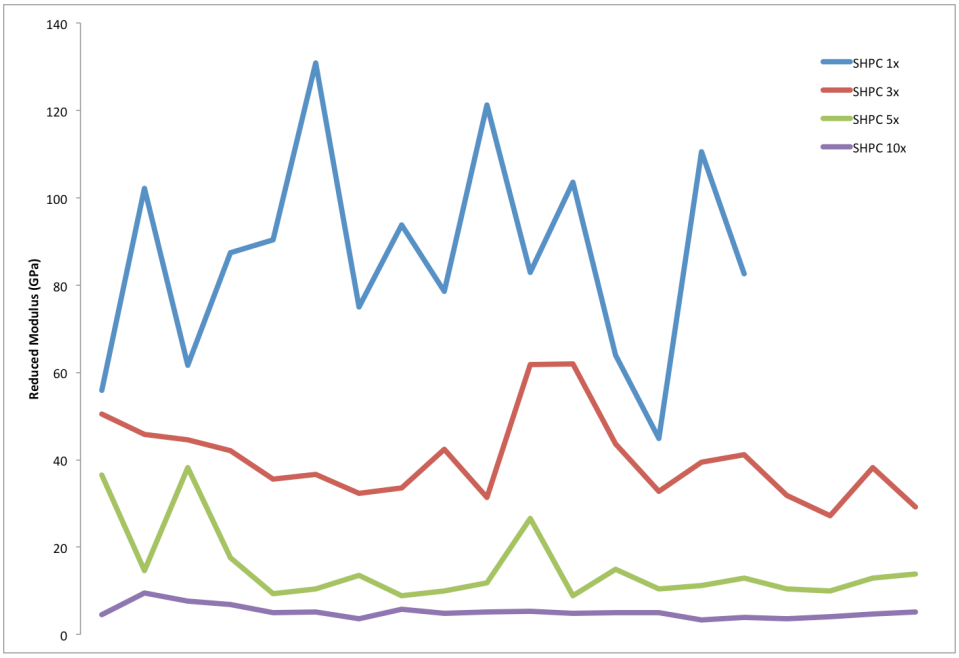


Figure 37: The reduced modulus obtained from nanoindentation on the SHPC coatings

VITA

Gimgun Loi was born on May 2nd, 1992 in Oslo, Norway. She moved to Knoxville, TN at the age of 8 and obtained a High School Degree from Bearden High School in May 2010. She then continued her studies at the University of Tennessee on a 5 year BS/MS program earning a Bachelor's of Science degree in Materials Science and Engineering in June 2014. She is diverse in her experience working on projects such as development of packaging of metal halide scintillators and development of biodegradable packaging using chitosan. She has extended her specialties to superhydrophobic research working to produce a marketable product in collaboration with Dr. Benson and Steve McNeany. She has submitted two invention disclosures and is aiming to pursue an engineering career in research and development.